Electronic Thesis and Dissertation Repository

8-18-2016 12:00 AM

Ultraprecise Single Point Inverted Cutting Strategies for Multi-axis Fabrication of Right Triangular Prismatic Retroreflectors

Benjamin W. Hamilton
The University of Western Ontario

Supervisor
Remus Tutunea-Fatan
The University of Western Ontario Joint Supervisor
Evgueni Bordatchev
The University of Western Ontario

Graduate Program in Mechanical and Materials Engineering
A thesis submitted in partial fulfillment of the requirements for the degree in Master of Engineering Science
© Benjamin W. Hamilton 2016

Follow this and additional works at: https://ir.lib.uwo.ca/etd

Part of the Manufacturing Commons

Recommended Citation

Abstract

The optical phenomenon of retroreflection (RR) is described as light rays contacting a surface and being redirected back to their originating source. While applications are many and varied, their primary focus is safety in low-light conditions, and the focus of this research is toward automotive applications. Few geometric shapes are capable of retroreflection. Among them are the lens-and-mirror, and cube corner geometry; however, the right triangular prism (RTP) has been introduced as a viable alternative. This study demonstrates a more efficient fabrication technology when compared to current industry practices.

The ultraprecise single point inverted cutting (USPIC) technology was envisioned as a combination of diamond turning and multi-axis machining. The unique cutting kinematics of USPIC required the development of dedicated tooling and a postprocessor for machine automation. Experimental results have demonstrated both the feasibility of this approach, and that RTP arrays fabricated by this technology outperform those fabricated through conventional means.

Keywords

i

Co-Authorship Statement

Chapter 1:   Benjamin Hamilton – wrote manuscript.

Chapter 2:   Benjamin Hamilton – designed study, performed experiments, wrote manuscript; Sama Hussein – performed optical simulations, analyzed/interpreted data; Remus Tutunea-Fatan – designed study, revised manuscript; Evgueni Bordatchev – designed study, revised manuscript.

Chapter 3:   Benjamin Hamilton – designed study, performed experiments, wrote manuscript; Sama Hussein – performed optical simulations, analyzed/interpreted data, contributed to the manuscript; Remus Tutunea-Fatan – designed study, revised manuscript; Evgueni Bordatchev – designed study, revised manuscript.

Chapter 4:   Benjamin Hamilton – designed study, performed experiments, wrote manuscript; Sama Hussein – performed optical simulations, analyzed/interpreted data, contributed to the manuscript; Nicolas Milliken – performed microscopy measurements, analyzed/interpreted data; Remus Tutunea-Fatan – designed study, revised manuscript; Evgueni Bordatchev – designed study, revised manuscript.

Chapter 5:   Benjamin Hamilton – designed study, performed machining experiments, wrote manuscript; Sama Hussein – performed optical simulation, analyzed/interpreted data, contributed to the manuscript; Nicolas Milliken – contributed to machining experiments; Remus Tutunea-Fatan – designed study, revised manuscript; Evgueni Bordatchev – designed study, revised manuscript.

Chapter 6:   Benjamin Hamilton – wrote manuscript.

Acknowledgments

Dedication

To the Creator of all I know; the good and faithful One.

"And whatever you do, whether in
word or deed, do it all in the name
of the Lord Jesus, giving thanks to
God the Father through him."

Table of Contents

List of Tables

List of Figures

List of Abbreviations

3D	Three Dimensional
CAD	Computer Aided Design
CAM	Computer Aided Manufacturing
CC	Cube Corner
CL	Cutter Location Data
CNC	Computer Numeric Control
DMC	Diamond Micro Chiseling
DMD	Digital Micromirror Device
FDOC	Finishing Depth of Cut
ICC	Inverted Cube Corner
LED	Light Emitting Diode
MCS	Machine Coordinate System
PMAC	Programmable Multi Axis Controller
PMMA	Polymethyl Methacrylate
RDOC	Roughing Depth of Cut
RR	Retroreflector
RRE	Retroreflective Efficiency
RTP	Right Triangular Prism
SEM	Scanning Electron Microscope
TIR	Total Internal Reflection
USPIC	Ultraprecise Single Point Inverted Cutting
UV	Ultraviolet
WCS	Work Coordinate System

CHAPTER 1

Introduction

1.1   Micro-optics

By broad definition, the field of micro-optics is related to the engineering of components with feature sizes in the micrometer (10^{-6} m) range which serve to manipulate light (Zappe, 2010). Thanks to advances in manufacturing technology, most notably in the field of semiconductor technology, the miniaturization of optical components has been a developing field since the early 1980s. Literature suggests that the term "micro-optics" was first used by Drs. Teiji Uchuda and Ichiro Kitano in the late 1960s (Sinzinger and Jahns, 2005). But it was not until 1982 that the term was applied to a specific component when Kenicha Iga *et al.* developed a micro-lens for use in optical fiber communications (Iga *et al.*, 1982; Zappe, 2010). The 1.0 mm diameter lenses had a focal length of 2.5–3 mm and were fabricated with a technique known as electromigration which is not typically understood as a fabrication technique. It is rather a mechanism which negatively affects the reliability of integrated circuits, and is caused by a momentum transfer from electrons, which constitute the flow of electricity, to the atoms of the conducting media – causing them to be displaced and the flow of electrons disrupted (Baldini *et al.*, 1993; Lim *et al.*, 2013).

Micro-lenses were first fabricated with electromigration because the well established fabrication procedures (*i.e.* cutting, grinding and polishing) were not applicable to lenses with a diameter of 1 mm or less (Zappe, 2010). Electromigration, and other techniques which will be discussed, made it possible to fabricate optical components which otherwise would not have been realized.

Applications for micro-optical devices range from medicine to entertainment, and appear in many of our everyday lives. One such application is the Digital Micromirror

Device (DMD), which was first used in digital projectors in 1996 (Zappe, 2010). It is comprised of many small mirrors which are each mechanically actuated to one of two positions. Each 16×16 µm mirror is fixed to a hinge and assembled into array sizes as large as 1280×1024 pixels (1.31 million individual mirrors) on a silicon chip. The position of each mirror is controlled electrostatically to either the "on" or "off" position. In the "on" position the mirror reflects light from a bulb to the projector lens which makes the pixel appear bright, otherwise the mirror reflects light away from the lens and the pixel appears dark. The relative brightness of each pixel is controlled by the length of time its corresponding mirror is held in the "on" position. Again, this technology was only made possible through advances in semiconductor technology (Lee, 2013).

Micro-optical components can be classified according to whether they are passive or active. Passive components interact with light and include mirrors, lenses, optical fibers, and diffraction gratings. These components do not require the addition of energy for their function; however, active components require or produce energy – usually electrical. Light emitting diodes (LEDs), photodetectors, and liquid crystals are each classified as active components (Sinzinger and Jahns, 2005; Zappe, 2010). These are just a few of the components that constitute the broad field of micro-optics, and the methods of manufacturing these components are as broad and technically advanced as the field itself (Sinzinger and Jahns, 2005; Kemme, 2010). While a comprehensive discussion on these methods is not feasible within the introduction of this thesis, a few of the more relevant techniques will be introduced.

Since the first micro-lenses were fabricated through electromigration, many other techniques have been developed and applied with varying results, but these generally draw

from a limited number of fundamental principles. One of these principles being surface tension in which a volume of fluid seeks to form a shape of least energy – a sphere. This phenomenon can be seen after a rainfall as drops of water form hemispherical shapes on windows and other low-wetting surfaces. Many of the fabrication techniques for micro-lenses rely on the principle of surface tension, such as the melted photoresist lens, or reflow lens (Figure 1.1). In this technique a small cylinder of polymer is heated above its glass transition temperature and begins to flow as a fluid. Surface tension causes the shape of the polymer to take on a hemispherical shape with a radius of curvature, r_c, and focal length determined by $f = {r_c}/{n-1}$, where n is the refractive index of the lens material (O'Neill *et al.*, 2004; Sinzinger and Jahns, 2005).
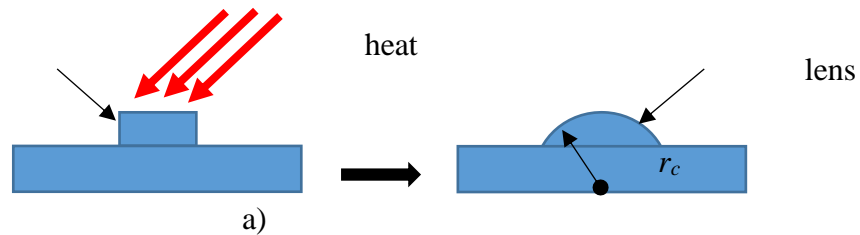
Figure 1.1 Reflow lens process: a) melting polymer cylinders, and b) resulting refractive lens

In more recent work, micro-lenses have been fabricated with the use of lasers on soda-lime glass substrates (Delgado *et al.*, 2016). This is a two-step process consisting of direct-writing lens "posts" in the glass, followed by a post-thermal treatment which gives the lens its shape and functionality. Delgado *et al.* fabricated an array of lenses with a diameter and period of 60 µm and 90 µm, respectively. The direct-writing step was carried out with precision laser ablation where a pulsed Ytterbium femtosecond laser removes material from a substrate by evaporation. The material is removed such that a cylindrical post

remains with diameter and height of 60 and 15 µm, respectively. The post-thermal treatment is done with a CO_2 laser and assisted by a roller furnace for improved process control. Similar to the reflow process in Figure 1.1, the glass cylinder is brought to the melting temperature where it begins to flow as a liquid. In this phase, surface tension governs the spherical shape of the lens. When the glass is allowed to cool back to its solid-state, it retains its lens-like shape.

Rapid prototyping techniques have also been used for the fabrication of micro-optical components. One particular technique is stereolithography, where a near-infrared laser is used to set a photopolymer which cures in UV light. Two separate lasers are pointed such that the two beams intersect at a controlled point. It is here that the two beams have enough energy to cure the UV photopolymer while leaving the rest of the polymer in its liquid state. 3D structures designed in a CAD environment are built up in layers as small as 0.2 µm with comparable XY resolutions. The result is a micro-manufacturing technique that has been extensively applied to the field of micro-optics (Maruo, 2008).

At the beginning of this discussion it was mentioned that the field of micro-optics would not have advanced as far as it has if it were not for the parallel advancement of semiconductor technology. While this remains true, recent advances in precision manufacturing with 5-axis machine tools have allowed for the fabrication of micro-optical components. These precision machines are capable of achieving optical surface finishes of $R_a < 10$ nm, and the linear axes have resolutions as low as 10 nm with a positional accuracy of ±250 nm (Bordatchev, 2013). They have been used in many applications, including the fabrication of high-quality diffraction gratings for state-of-the-art spectrometers (Davies *et al.*, 2012).

1.2   Retroreflectors

The retroreflector is classified as a passive optical device that is able to return an incident light beam back to its source through a range of incidence angles (Nilsen and Lu, 2004). It differs from typical reflection which returns light back to the source only at a zero angle of incidence (Figure 1.2a). Retroreflection also differentiates itself from diffuse scattering in that a large percentage of the incident light is returned to the source (*i.e.* minimal scattering). Applications for retroreflectors are primarily related to safety in low light situations: automotive lighting, road signs and surfaces, bicycles, and safety clothing. Retroreflectors have also been used for optical communication and radar detection (Park *et al.*, 2012).
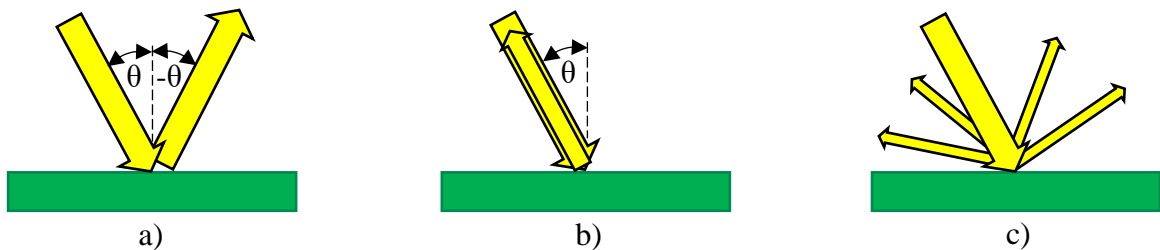
Figure 1.2 a) reflection, b) retroreflection, and c) diffuse scattering

The Retroreflection effect of dew covered grass was first modeled by Lommel in 1874 (Nilsen and Lu, 2004). He proposed that the spherical nature of the water droplet focused incoming light onto the surface of the grass supporting the droplet. The light is then reflected and the droplet again focuses the light toward the source. A person standing with the morning sun to their back will see that the edge of the shadow cast by their head glows as the sunlight is retroreflected. It should be stressed that true retroreflection requires that the incident and returned light are parallel to one another. For this reason, it is the edge of

the shadow that glows, which represents the area where the rays of incident light have the least parallel distance from the eyes of the viewer (Figure 1.3).
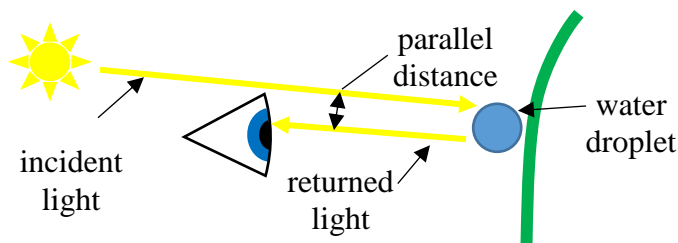
Figure 1.3 Retroreflection of dew droplets

The model proposed by Lommel has been categorized as a lens-and-mirror retroreflector. It is also known as a "cat's eye" RR because of the way many animals, cats included, have eyes that reflect light as a result of a reflective layer behind the retina which allows for light to pass through the retina twice – increasing their ability to see at night (Nilsen and Lu, 2004). This natural phenomenon has been reproduced using a transparent sphere with a reflective coating applied to the back. In order to ensure the light is focused onto the reflective coating, it is necessary that the sphere be made of a material with a refractive index of 2.0.

Another important RR category is the cube corner, which received its name based on the fact that it is composed of two or three sides of a cube sharing a common vertex. While the geometry of each side (*i.e.* facet) can be somewhat arbitrary, it is necessary that the facets are planar and mutually orthogonal for proper functionality. If the angle between facets deviates from 90°, divergence is introduced to the retroreflector, and its effectiveness over long distances will be diminished. Therefore, manufacturers must adhere to tight angular tolerances.

There are three basic types of cube corner RRs based on the number and shape of their facets (Hussein *et al.*, 2016). Notice in Figure 1.4 below that RRs with three facets are either designated as triangular or hexagonal, and those with two facets have been named right triangular prisms (RTP).

hexagonal

triangular
aperture

a)

b)
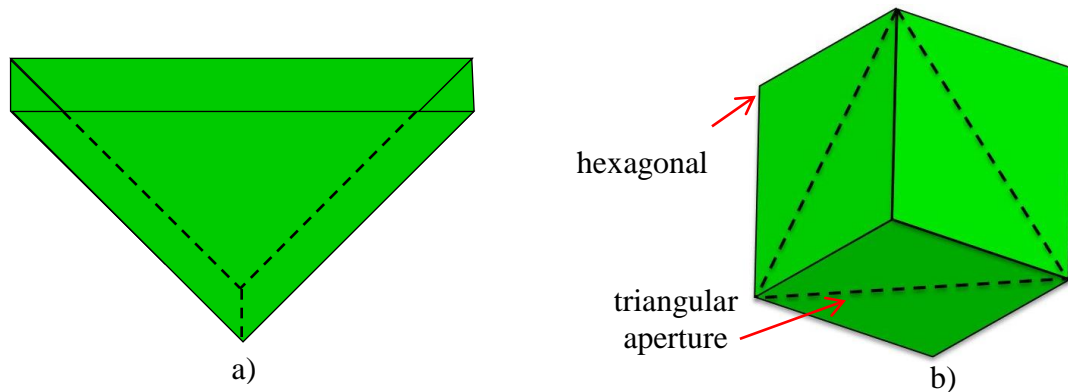
Figure 1.4 Cube corner retroreflectors with: a) two facets, and b) three facets

The term aperture stems from the shape of the perimeter formed by the structure when viewed along its axis of operation. In Figure 1.4b, a hexagonal aperture is formed by a three-sided cube corner with square facets, while a triangular aperture is formed by a cube corner with triangular facets. Following this principle, the RTP has a rectangular aperture with no specific aspect ratio required by the geometry. The overall size of these structures can either be micro or macro, and it is the specific application which determines the permissible scale.

Each of these structures share a common function; however, their operating characteristics, and specific applications, differ greatly. The lens-and-mirror type of retroreflector is widely used in reflective clothing worn by road workers, and the reflective paint used to mark roadways because the small, spherical, glass beads used in the paint are

economical to manufacture and do not require a specific orientation (MnDOT, 2015). Although the retroreflective efficiency of a single bead is quite high, the packing factor of an array of beads reduces the overall efficiency of an area covered by the paint (Nilsen and Lu, 2004). For this reason, the lens-and-mirror RR is a low-cost solution for many applications.

The differences in geometry between the hexagonal and triangular aperture cube corner RRs also lead to differences in their retroreflective characteristics and ease of manufacturing. The triangular aperture has a peak efficiency of 67% while the hexagonal aperture returns 100% of the light at a zero incidence angle (Seward and Cort, 1999). Furthermore, an array of triangular structures has a continuous toolpath which lends itself to more cost effective manufacturing procedures when compared to an array of hexagonal structures (Brinksmeier *et al.*, 2008). Therefore, the hexagonal aperture is used in applications where safety takes precedence over cost.

Likely one of largest applications of these structures is the automotive industry, where arrays of hexagonal structures are manufactured into the lenses of side markers and taillights as a means of increasing driver safety through visibility. When a vehicle is parked at night on the side of the road, oncoming traffic may not see the vehicle with enough time to safely maneuver around it. With the addition of RRs to the parked vehicle, it is more distinguishable to other drivers when the light from their headlights is returned to their eyes by the RRs on the parked vehicle.

1.3   Motivation

In typical automotive applications, structure sizes are about 2–3 mm and array sizes sometimes larger than 100 mm^2, requiring thousands of individual structures. The manufacturing technique used for these arrays, which will be fully described in subsequent chapters, was developed in the 1970s and is still in use today (Van Arnam, 1978). Arrays are manufactured in batches using injection moulding techniques which can produce parts with cycle times of less than one minute. While this is a cost-effective approach for producing the functional RR arrays, it is improving the technique used to fabricate the moulds that should be addressed. The minimum possible structure size is about 1 mm and many time intensive steps are required to fabricate the mould which ultimately lead to it being a costly technique, prone to error. Yuan *et al.* addressed the current size limitations by applying the Reactive Ion Etching Technique developed for semiconductor micro-fabrication (Yuan *et al.*, 2002). They were able to produce cube corner arrays with 10 µm structure sizes, but the RR functionality of the structures was not stated.

In more recent work precision 5-axis machine tools have been used to create arrays of hexagonal aperture cube corner RRs (Brinksmeier *et al.*, 2012). A 10×10 mm planar array of 150 µm structures was created using a specialized procedure. The resulting surface finish of the facets was within the optical requirements (*i.e.* $R_a < 10$ nm), and the optical performance of the array was evaluated using a reflection measurement system. This procedure requires an ultraprecise machine tool and diamond tooling to achieve the geometrical accuracy achieved in testing, but the result is a procedure which enables manufacturers to produce a mould for the recreation of optically functional hexagonal RR structures with dimensions not previously realized with the former technique.

1.4   Purpose of the Thesis

This research was conducted in collaboration with the National Research Council of Canada (NRC) – the Government of Canada's premier research and technology organization. Working alongside Canadian businesses, they are focused on developing new technologies that will keep Canadian industry competitive on the global market. One of the goals of the Automotive and Surface Transportation division of NRC is to develop advanced manufacturing technologies for the Canadian automotive parts industry (NRC, 2016). This thesis has partnered with that goal and seeks to develop a technology to improve the current procedure for the manufacturing of automotive retroreflective optics.

The following chapters of this thesis contribute to the overall goal of developing a new and innovative manufacturing procedure. The second chapter seeks to introduce the need for a method of fabricating right triangular prism retroreflectors. The third chapter evaluates the optical performance and geometrical accuracy of the method developed, and suggests the steps that should be taken to improve upon these results. The fourth chapter implements these suggestions and evaluates their results, while the fifth chapter offers a detailed discussion of how the improvements were realized. The final chapter of this thesis proposes steps to be taken in order to further develop this manufacturing procedure.

1.5   Thesis Contributions

The widespread application of retroreflectors has required the development of specific manufacturing techniques. Whether the retroreflective structures are macro or micro-sized, their manufacturing techniques are well-documented in literature (Van Arnam, 1978; Yuan *et al.*, 2002; Brinksmeier *et al.*, 2012). The techniques applied to macro retroreflectors

(larger than 1 mm) require specially designed procedures, yet still make use of standard machine tools; however, the techniques applied to micro retroreflectors with more complex geometry (*i.e.* hexagonal cube corners) have traditionally made use of technology developed for semiconductors. Recent developments in ultraprecise machine tools have enabled the development of cutting techniques and toolpaths applicable to hexagonal cube corners. At the beginning of this research, there were no documented techniques for the fabrication of the right triangular prism geometry. This thesis will contribute to that knowledge gap by developing such a technique applicable to the ultraprecise machine tools available today.

1.6   Overview of Thesis

The second chapter of this thesis introduces the need for a manufacturing technique applicable to micro-sized right triangular prism (RTP) retroreflectors. The bidirectional Ultraprecise Single Point Inverted Cutting technique (USPIC) was developed as an alternative to the common pin-bundling technique, and is capable of producing planar arrays of RTP structures in a brick-like pattern. Verification of this technique was completed on a PMMA (polymethyl methacrylate) sample, which allowed for the immediate evaluation of the optical performance of the retroreflective characteristics of the array. While the chapter is not presented in chronological order with the remaining chapters, it was written in response to criticism regarding the novelty of the cutting technique – the issue being a lack of clarity in the other chapters.

Chapter three describes and implements the first iteration of the USPIC technique. The effects of a geometric artifact, resulting from the common pin-bundling technique, is simulated and compared directly to the RTP structure, fabricated with the USPIC

technique, that does not have such defects. The strategy is implemented directly on a PMMA sample, which allows for direct evaluation of the optical performance without having to reproduce the array using moulding techniques. The cutting strategy requires that the tool be engaged in the material in two different orientations – one for each facet, and the resulting surface finish is analyzed qualitatively with the use of SEM images, because the complex geometry does not allow for common methods of measuring surface roughness.

In chapter four, a CAD based macro is introduced which reduces the time required for simulating the optical performance of RTP arrays, and aids visualization. The primary objective of the chapter is to modify the cutting kinematics and geometry in an effort to improve the resulting surface finish. This required the full functionality of the 5-axis ultraprecise machine tool, necessitating the development of an inverse kinematic model and postprocessor. Experimental validation was again carried out on a PMMA sample for the purpose of direct optical evaluation of the optical performance, and comparison to previous results. The final result of this chapter is an optically functional retroreflective array.

The fifth and final chapter introducing new content is a more detailed description of the postprocessor briefly discussed in the previous chapter. The block diagram is presented along with the equations used to calculate the machining coordinates of the USPIC method. An improved kinematic model, applicable to arrays of RTP structures, is introduced. Further experimental validation is carried out while small changes are made to the cutting geometry for the purpose of enhancing the surface finish of the cut facets, thereby increasing the optical functionality of the array.

1.7   References

Baldini, G. L., Demunari, I., Scorzoni, A. & Fantini, F. 1993. Electromigration in Thin-Films for Microelectronics. *Microelectronics and Reliability,* **33**, 1779–1805.

Bordatchev, E. V. 2013. Demonstration of Advanced Capabilities of 5-Axis Micromilling: Geometries with High Aspect Ratio and/or Optical Surface Quality. *International Conference on Micromanufacturing.* Victoria.

Brinksmeier, E., Gläbe, R. & Flucke, C. 2008. Manufacturing of molds for replication of micro cube corner retroreflectors. *Production Engineering,* **2**, 33–38.

Brinksmeier, E., Glabe, R. & Schonemann, L. 2012. Diamond Micro Chiseling of large-scale retroreflective arrays. *Precision Engineering-Journal of the International Societies for Precision Engineering and Nanotechnology,* **36**, 650–657.

Davies, M. A., Dutterer, B. S., Suleski, T. J., Silny, J. F. & Kim, E. D. 2012. Diamond machining of diffraction gratings for imaging spectrometers. *Precision Engineering-Journal of the International Societies for Precision Engineering and Nanotechnology,* **36**, 334–338.

Delgado, T., Nieto, D. & Flores-Arias, M. T. 2016. Soda-lime glass microlens arrays fabricated by laser: Comparison between a nanosecond and a femtosecond IR pulsed laser. *Optics and Lasers in Engineering,* **86**, 29–37.

Hussein, S., Hamilton, B., Tutunea-Fatan, O. R. & Bordatchev, E. V. 2016. Novel Retroreflective Micro-Optical Structure for Automotive Lighting Applications. *SAE International Journal of Passenger Cars – Mechanical Systems,* **9**.

Iga, K., Oikawa, M., Misawa, S., Banno, J. & Kokubun, Y. 1982. Stacked Planar Optics - an Application of the Planar Microlens. *Applied Optics,* **21**, 3456–3460.

Kemme, S. A. 2010. *Microoptics and Nanooptics Fabrication,* Boca Raton, Taylor & Francis Group.

Lee, B. 2013. DMD 101: Introduction to Digital Micromirror Device (DMD) Technology.

Lim, M. K., Chouliaras, V. A., Gan, C. L. & Dwyer, V. M. 2013. Bidirectional electromigration failure. *Microelectronics Reliability,* **53**, 1261–1265.

Maruo, S. 2008. Optically Driven Micromachines for Biochip Application. *In:* OHNO, K., TANAKA, M., TAKEDA, J. & KAWAZOE, Y. (eds.) *Nano- and Micromaterials.* Berlin, Heidelberg: Springer Berlin Heidelberg.

MnDOT. 2015. MnDOT Pavement Marking Field Guide. Available: http://www.dot.state.mn.us/trafficeng/pavement/doc-storage/mndotpavementmarkingfieldguide.pdf [Accessed July 13, 2016].

Nilsen, R. B. & Lu, X. J. 2004. Retroreflection technology. *Optics and Photonics for Counterterrorism and Crime Fighting,* **5616**, 47–60.

NRC. 2016. *National Research Council Canada* [Online]. Available: http://www.nrc-cnrc.gc.ca/eng/rd/ast/index.html [Accessed July 15 2016].

O'Neill, F. T., Walsh, C. R. & Sheridan, J. T. 2004. Photoresist reflow method of microlens production: Modeling and fabrication techniques. *Photon Management,* **5456**, 197–208.

Park, J., Won, J., Kim, D., Jo, M. S. & Park, J. Y. 2012. Piezoelectrically operated MEMS corner cube retroreflector for optical communications. *Journal of Micromechanics and Microengineering,* **22**.

Seward, G. H. & Cort, P. S. 1999. Measurement and characterization of angular reflectance for cube-corners and microspheres. *Optical Engineering,* **38**, 164–169.

Sinzinger, S. & Jahns, J. 2005. Microoptics. *Microoptics.* Wiley-VCH Verlag GmbH & Co. KGaA.

Van Arnam, D. 1978. *Method for Forming Retroreflective Sheeting*. U.S. patent application 4243618. January 6, 1981.

Yuan, J. H., Chang, S. J., Li, S. M. & Zhang, Y. X. 2002. Design and fabrication of micro-cube-corner array retro-reflectors. *Optics Communications,* **209**, 75–83.

Zappe, H. 2010. *Fundamentals of Micro-Optics,* Cambridge, Cambridge University Press.

CHAPTER 2

Enhanced Bidirectional Fabrication of
Right Triangular Prismatic Retroreflectors

2.1   Introduction

A retroreflector (RR) is a passive optical element with the primary function of returning

incident light back to its originating source (Figure 2.1). Retroreflection differentiates itself

from specular reflection in that light is returned through a range of incident angles. While

the applications of these optical structures are widespread, the primary focus of this paper

will be automotive lighting applications in which RRs are meant to supplement the vehicle

occupant safety by increasing the visibility of the vehicle to the surrounding traffic.
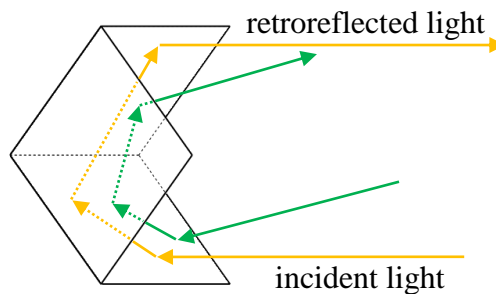
Figure 2.1 Cube corner retroreflective element

There are two basic classifications of retroreflective structures: lens-and-mirror, and cube

corner. The cube corner structure is characterized by a superior retroreflective ability across

a wide range of incidence angles. It derives its name as a result of being comprised of three

faces of a cube that are mutually orthogonal and share a common vertex. The faces can

either be square, as depicted in Figure 2.1, or triangular, and the shape determines the

cross–sectional area, retroreflective characteristics, and ease of manufacturing. The square

sided structure has a hexagonal cross-section and higher efficiency when compared to the

structure with a triangular aperture. For this reason, the structure primarily used in

automotive applications is the hexagonal cube corner. Nevertheless, manufacturing arrays

of these structures, necessary for automotive applications, is time consuming because of

the geometry's sharp 90° concave corners, and the non-continuous toolpaths, both of which contribute to rotating tools not being directly applicable.

Instead, manufacturers developed a technology in the late 1970s in order to produce the dies necessary for injection moulding of these components (Van Arnam, 1978). The pin-bundling technique involves the use of individual pins, each with a single "negative" RR structure machined and lapped at the "forming end" of the pin (Figure 2.2). The surface finish of the machined structure must be at least $R_a = 10$ nm to achieve sufficient optical functionality. Without an optical quality finish, the structure will scatter more light than is permissible. Each pin is then bundled into an array and electroplated with nickel. The electroform is then used as a cavity insert for the injection moulding die. Electroforming is a necessary step to replicating the geometry of the pins, because the final geometry of the functional part should be that of the pins, not their "mirror". The electroform allows for an accurate mould of the pins to be made; however, it is a time consuming process.

Single pin   Pin array
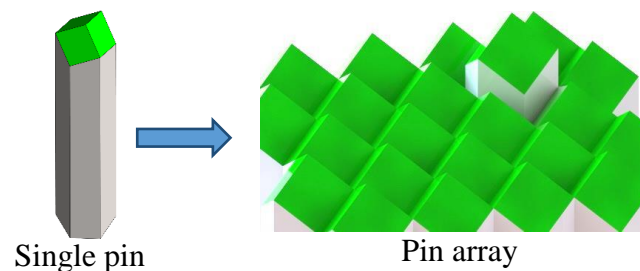
Figure 2.2 Pin-bundling technology

Typical structure sizes for automotive applications are about 2–3 mm and an array may have a surface area of 100 mm^2. Therefore, many thousands of pins are required for this technique. Also, the number of pins necessary for a given array is inversely proportionate to the individual structure size – as the structure size is reduced, the number

of pins required for a given surface area increases. Due partly to this, the pin-bundling technique is limited to structure sizes of about 1 mm.

The placement of pins on non-flat or flat and inclined surfaces leads to the formation of manufacturing artifacts called "pockets" (Figure 2.3) whose role on the optical performance of the RRs is rather unclear at this time.
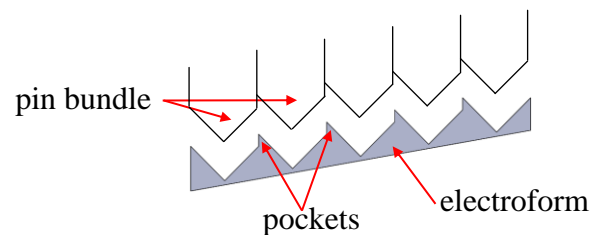
Figure 2.3 Manufacturing artifacts as a result of pin-bundling

Extensive research efforts were recently made to reduce the overall manufacturing time associated with the pin-bundling technology that requires in excess of hundreds of hours per insert, particularly in the case of automotive lighting components characterized by a complex freeform shape. For this purpose, Diamond Micro Chiseling (DMC) was identified as a viable alternative to pin-bundling (Brinksmeier *et al.*, 2008; Brinksmeier *et al.*, 2012b; Hamilton *et al.*, 2016a). DMC has also been utilized to fabricate structure sizes as small as 150 µm.

The switch from pin-bundling/forming to material removal/machining technologies enables a greater flexibility in terms of RR geometry and – when accompanied by optimized cutting strategies – an increased productivity. It is important to note again that the nature of the geometry necessary for RR prevents the use of classical tool path planning strategies associated with milling operations (Brinksmeier *et al.*, 2012a).

To date, diamond microchiseling technology was developed with a focus on the hexagonal cube corner RR geometry presented in Figure 2.1 & Figure 2.2 that was cut in a flat and horizontal base surface. This technology allows for direct machining of the injection moulding die by means of a V-shaped diamond tool whose motions are controlled by an ultraprecise five-axis micromachine tool. The diamond tool cuts each RR structure in multiple layers in order to improve the final surface finish and reduce tool wear.

In a further development of the microchiseling technology, ultraprecise single point inverted cutting will be presented in this study as a possibility to generate – without manufacturing artifacts – RRs characterized by right triangular prismatic geometries.

2.2   Geometry and Optical Performance of Right Triangular Prismatic RRs

Retroreflectors are generally classified according to the shape of their aperture as well as the number of facets involved in retroreflection. The right triangular prismatic (RTP) geometry is characterized by a rectangular aperture through which the incoming light rays enter and later exit, as well as two rectangular facets which reflect light through total internal reflection (Figure 2.4a). Unlike the cube corner geometry, the aperture of the RTP is not limited to a single aspect ratio, and while different geometric combinations can be imagined, the current study will be focused on a simple square aperture, isosceles form ($\beta = 45°$). At this angle, the axis of operation is normal to the surface of the structure.

The RTP geometry analyzed in this work was rarely – if ever – part of the taxonomy of retroreflectors since it was not fabricated before and as such its practical applicability was rather unclear. Recent simulation studies have shown that the retroreflective efficiency

of the RTP is comparable to the ubiquitous hexagonal cube corner geometry through a large range of incidence angles and outperforms it at incidence angles of less than four degrees (Hussein *et al.*, 2016).

a)

b)
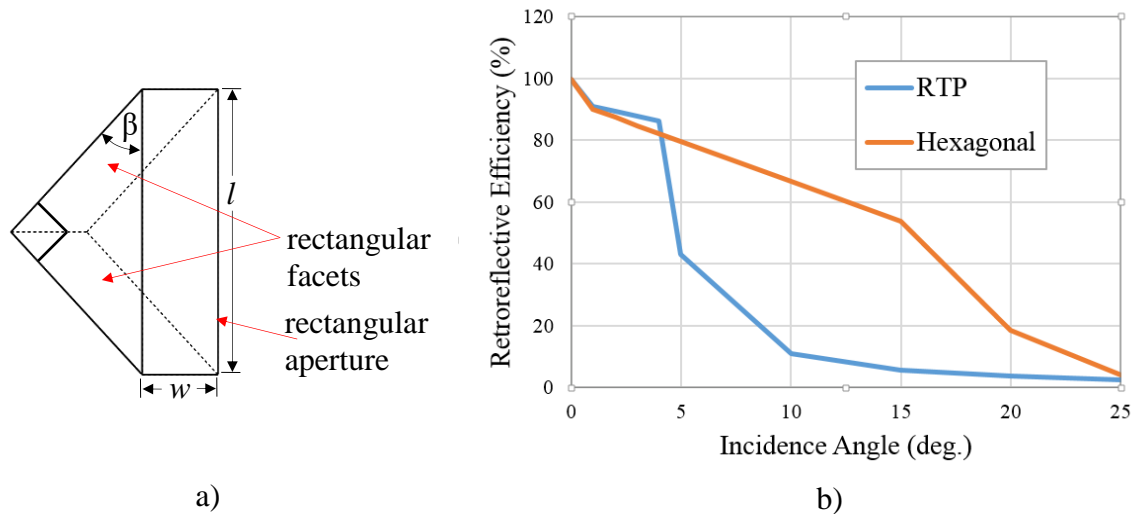
Figure 2.4 a) principal geometric parameters of an RTP, and b) retroreflective characteristics of RTP and hexagonal

2.3   Diamond Micro Chiseling

In order to achieve geometric accuracy and optical functionality, the hexagonal cube corner RRs directly machined with the Diamond microchiseling process have made use of an ultraprecise five-axis CNC machine tool and diamond tooling. The geometry of the diamond tool resembles that of a 50° V-shaped turning tool, yet is specific to the DMC process (Figure 2.5). The tool is aligned in the machine such that the conventional clearance and rake faces have been switched and therefore the tool geometry is different. The tool features a 22° rake angle and the clearance face has an angle of 2–3° ground into it (Brinksmeier *et al.*, 2012a).
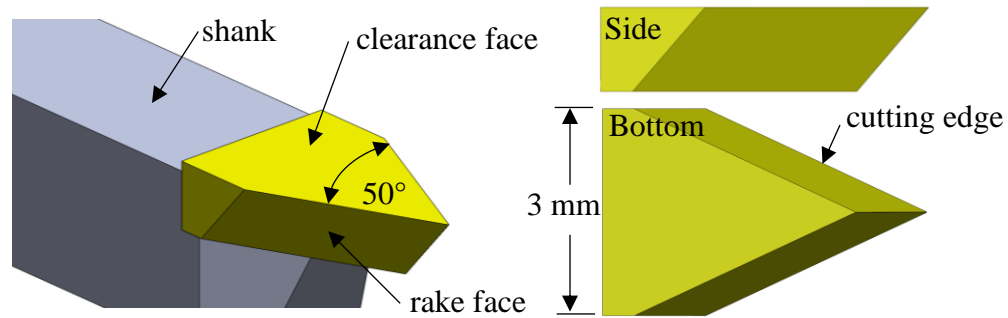
Figure 2.5 Geometry of the Diamond Micro Chiseling tool. Adapted from Brinksmeier *et al., 2012a*.

The two rotary axes of the five-axis machine tool are required for the alignment of the tool with the facets of the to-be-cut structure. The machine used in the DMC process has the B-axis connected to the spindle and the C-axis connected to the workpiece. This type of machine is known as a head/table tilting machine, because the head and table are each equipped with a rotary axis.

The cutting process follows a sequence of motions whereby layers of material are removed one-by-one. The first step is to align the clearance face of the tool with the plane of the facet to be cut. From this position, the nose of the tool is moved linearly along the edge of the facet in a two-step process: plunging along the first edge to the apex, followed by retracting along the second edge (Figure 2.6). In this V-motion, a single facet of the hexagonal cube corner is completed. The remaining two facets of the structure are completed following the same sequence, after a 120° rotation of the C-axis to align the plane of the facet to be machined with the tool. This process of cutting and rotating is repeated for each facet of each structure in the array.
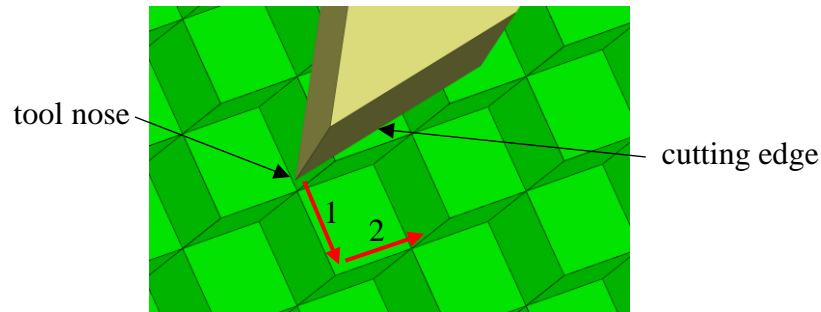
Figure 2.6 Cutting motions of a single facet. Adapted from Brinksmeier *et al., 2012a.*

2.4 Ultraprecise Single Point Inverted Cutting of Right Triangular Prisms

As illustrated by Figure 2.7, USPIC enables the fabrication of pocketless RTPs on flat but

inclined base surfaces.
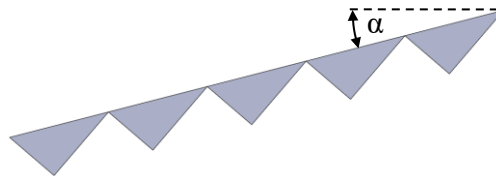
Figure 2.7 Pocketless array of right triangular prisms

Similar to microchiseling, USPIC requires a monocrystalline diamond, single point tool as

a prerequisite towards achieving an optical surface finish ($R_a < 10$ nm) that is mandatory

for adequate retroreflective efficiency. However, the geometry of the tool used in USPIC

operations has been tailored to RTP fabrication and therefore is different than that needed

for cube corner geometries. While the tool is of a custom design, its geometry is

comparable to a grooving tool used for turning operations (Figure 2.8). The wedge angle

was chosen to be 50° in order to prevent the chip from binding against the adjacent facet,

potentially damaging its surface finish, as the tool reaches the root of each cut. This angle

does however contribute to a large positive rake angle which, according to common theory,

is not ideal (Stephenson and Agapiou, 2006). Instead, it is a compromise necessitated by the RTP geometry. The width of the tool determines the smallest possible structure size, but larger structures are possible by effectively cutting multiple structures next to one another. For the purpose of this study, the tool width was chosen to be 450 µm.
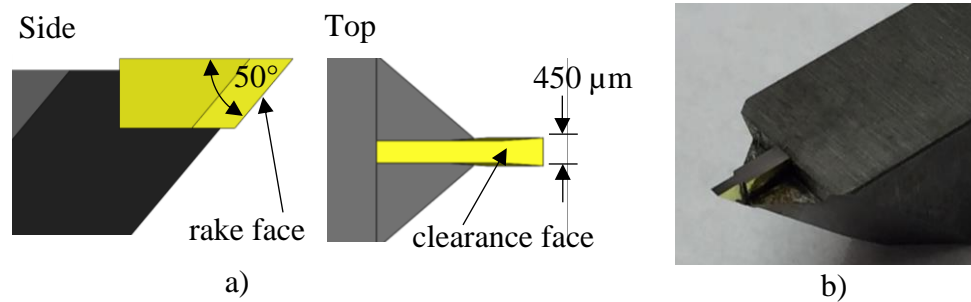
Figure 2.8 Geometry of USPIC tool: a) CAD model b) physical tool

2.4.1 Uni-directional Strategy

The kinematics of this strategy requires the cutting geometry to be quite different for each of the two facets of the RTP structure (Figure 2.9). The vertical facet engages the tool such that its cutting geometry is conducive to achieving an optical quality surface finish, while the horizontal facet engages the tool in a manner that results in a sub-optical surface finish. The vertical and horizontal cutting kinematics have been termed plunging and ploughing, respectively. Plough cutting is defined as cutting geometry where the clearance angle is at least 90°, resulting in a negative rake angle equal to or greater than the wedge angle. Alternatively, a plunge cut, has preferred cutting geometry with a small clearance angle and positive rake angle. Since the resulting surface directly contributes to the optical functionality, this strategy is insufficient for a finishing procedure; however, its high material removal rate is such that it remains applicable to roughing procedures where surface finish is not the principal priority.
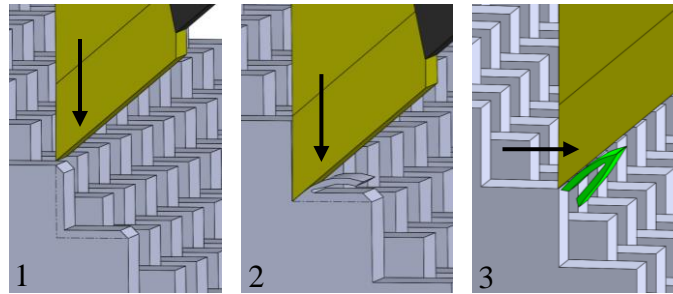
Figure 2.9 Uni-directional cutting strategy

2.4.2 Bi-directional Strategy

As suggested by Figure 2.10, the kinematics of the bi-directional strategy result in the optimal cutting geometry for both facets of the RTP; however, these cutting motions require the full functionality of a five-axis CNC machine center. The primary role of the two rotary axes is indexing/positioning in order to properly align the cutting tool with the RTP facets. This type of machining is also known as 3½½-axis machining, because the rotary axes are held stationary as the tool removes material (Chen *et al.*, 2003). In this bi-directional approach, the two active facets of the RTP are being cut alternatively, such that "ploughing" is no longer necessary since the entire RTP is generated by means of "plunging" motions. However, the relatively low traverse rate of the rotary axes reduces the material removal rate when compared to the uni-directional strategy, therefore its primary application should be as a finishing strategy in which the primary interest is achieving a surface finish of optical quality.
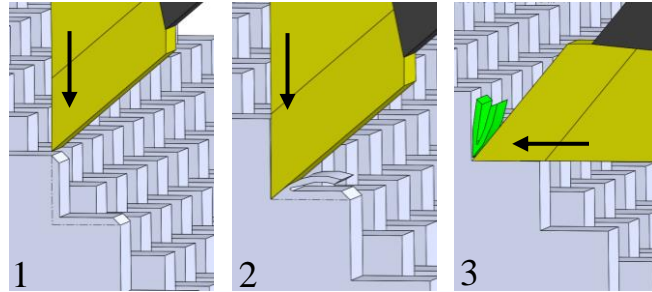
Figure 2.10 Bi-directional cutting strategy

The culmination of this discussion is a strategy in which an array of RTP structures are cut with separate roughing and finishing procedures. The uni-directional USPIC strategy has been used to rough-cut the structure, resulting in a near-complete geometry, while the bi-directional USPIC strategy has been applied as a finishing procedure. This strategy represents a further iteration of the original 3½½-axis cutting that was introduced in the past (Hamilton *et al.*, 2016b). And while many of the process setting and parameters were kept unchanged, a special calibration protocol has to be used to ensure the post-indexing parallelism between the RTP facet and the rake face of the diamond tool. The calibration procedure requires that the tool be aligned to an XYZ tolerance of ±1 µm for chips to be properly released from the workpiece throughout cutting.

2.5   Experimental Validation

Figure 2.11 shows a representative sample of a planar array of RTP structures that was cut in 0.5 mm thick PMMA. The array is composed of 601 structures, each characterized by the following dimensional parameters: $w = 450\,\mu m$, $l = 450\,\mu m$, and a surface finish $R_a < 90$ nm. Although preliminary inspection proves the optical functionality of the array, measurements have not been conducted in an effort to quantify these results.
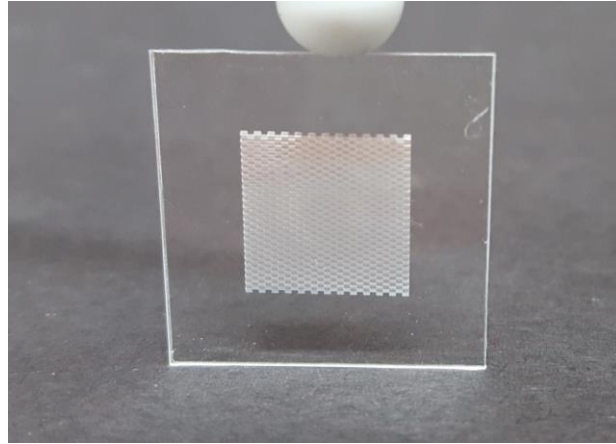
Figure 2.11 Fabricated array of RTP structures

2.6 Conclusions

The presented enhanced USPIC technique represents a viable option for the fabrication of the RTPs. It is important to note that while USPIC was developed as an alternative for mould fabrication, its use on PMMA enables the immediate validation of the optical performance of the generated RR arrays. Future efforts will be made toward improving surface finish of the reflective facets.

2.7 Acknowledgements

2.8   References

Brinksmeier, E., Gläbe, R. & Flucke, C. 2008. Manufacturing of molds for replication of micro cube corner retroreflectors. *Production Engineering,* **2**, 33–38.

Brinksmeier, E., Glabe, R. & Schonemann, L. 2012a. Diamond Micro Chiseling of large-scale retroreflective arrays. *Precision Engineering-Journal of the International Societies for Precision Engineering and Nanotechnology,* **36**, 650–657.

Brinksmeier, E., Gläbe, R. & Schönemann, L. 2012b. Review on diamond-machining processes for the generation of functional surface structures. *CIRP Journal of Manufacturing Science and Technology,* **5**, 1–7.

Chen, Z. Z. C., Dong, Z. M. & Vickers, G. W. 2003. Automated surface subdivision and tool path generation for 3 1/2 1/2-axis CNC machining of sculptured parts. *Computers in Industry,* **50**, 319–331.

Hamilton, B., Hussein, S., Tutunea-Fatan, O. R. & Bordatchev, E. V. 2016a. Fabrication of Right Triangular Prism Retroreflectors through Ultraprecise Single Point Inverted Cutting. *Manufacturing Science and Engineering Conference.* Blacksburg, Virginia.

Hamilton, B., Milliken, N., Hussein, S., Tutunea-Fatan, O. R. & Bordatchev, E. V. 2016b. Fabrication of Right Triangular Prism Retroreflectors through 3 1/2 1/2-Axis Ultraprecise Single Point Inverted Cutting. *Computer-Aided Design and Applications*.

Hussein, S., Hamilton, B., Tutunea-Fatan, O. R. & Bordatchev, E. V. 2016. Novel Retroreflective Micro-Optical Structure for Automotive Lighting Applications. *SAE International Journal of Passenger Cars – Mechanical Systems,* **9**.

Stephenson, D. & Agapiou, J. 2006. *Metal Cutting Theory and Practice 2nd Edition,* Boca Raton, Taylor and Francis.

Van Arnam, D. 1978. *Method for Forming Retroreflective Sheeting*. U.S. patent application 4243618. January 6, 1981.

CHAPTER 3

Fabrication of Right Triangular Prism Retroreflectors
through Ultraprecise Single Point Inverted Cutting

3.1   Overview

Retroreflectors (RR) represent optical elements whose primary functionality is to return incident light back to its originating source. While inverted cube corner (ICC) geometry constitutes the de facto standard in automotive lighting applications, other RR designs exist. Among them, right triangular prism (RTP) constitutes a viable alternative and therefore, the main intention of the present study was to demonstrate that a fabrication means other than the ineffective conventional pin-bundling technology is possible.

To address this, a new ultraprecise single point inverted cutting (SPIC) technology – envisioned as a virtual combination between diamond turning and five-axis machining – was introduced as a viable manufacturing option for the fabrication of the RTP RR arrays. While simulation results seem to suggest a slight optical superiority of the RTP RR arrays produced through conventional, rather than SPIC approaches, experimental results have demonstrated that fabricating RTP RR prototypes is not only possible, but it can yield better retroreflective efficiencies when compared to state-of-the-art ICC-based automotive retroreflectors.

3.2   Introduction

Retroreflectors (RRs) are passive optical components that have the ability to reflect a light beam back to its source through a range of incident angles deviating from the normal axis. There are three primary groups of retroreflectors: lens-and-mirror (or cat's eye), and inverted cube corner (ICC) (Figure 3.1). RRs are used in illumination and safety applications (i.e., automotive reflectors, road signs, safety clothing), as well as in communications systems (Seward and Cort, 1999).

When compared to the lens-and-mirror RR, cube corner RRs are characterized by higher efficiency, but the former allow for larger incident angles deviating from the normal axis (So *et al.*, 2002). Because of their superior efficiency (i.e., luminance), this study will present a new cutting technology which was used to fabricate arrays of RR elements that are functionally similar to CC RRs.
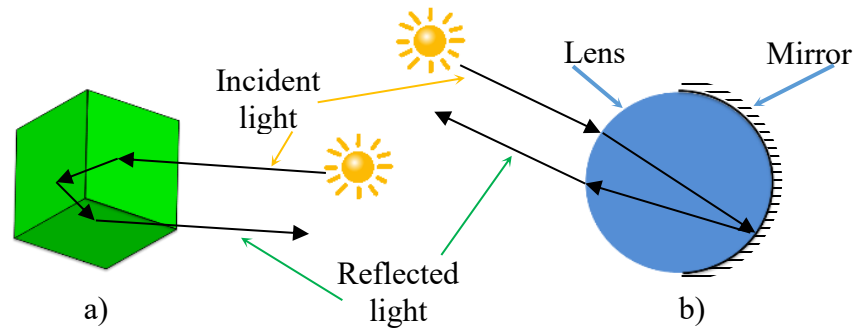
Figure 3.1 Typical RR elements: a) cube corner, and b) lens-and-mirror

The new RR geometry to be demonstrated in the context of the present work was recently introduced and termed as right triangular prism (RTP) (Hussein *et al.*, 2016). In this regard, it can be mentioned here that a retroreflective array is comprised of a number of elements that effectively form a structured surface characterized by incoming light returning/reflecting capabilities.

3.3 Design and Fabrication of ICC RRs for Automotive Lighting Applications

The geometry of the cube corner RR can be described by means of two or three sides of a cube that share a common vertex. Because the CC RR geometry is derived from a cube, its facets are mutually orthogonal and this is in fact a prerequisite of its retroreflectivity. If the angle between two adjacent faces deviates from 90°, the efficiency of the retroreflector will be diminished as a result of divergence, in a sense that the incident and reflected beams

will no longer be parallel (Seward and Cort, 1999). However, automotive lighting manufacturers prefer to introduce a certain level of divergence in their retroreflectors, particularly because in many traffic applications the source and viewer are often separated by a certain distance (Seward and Cort, 1999).

Three main types of retroreflectors have been identified so far with respect to the shape of aperture as well as the number of reflective facets participating in retroreflection: i) right triangular prism (RTP) with rectangular aperture and two reflective facets, ii) CC with a triangular aperture and three reflective facets, and iii) CC with a hexagonal aperture and three reflective facets (Figure 3.2) (Hussein *et al.*, 2016).
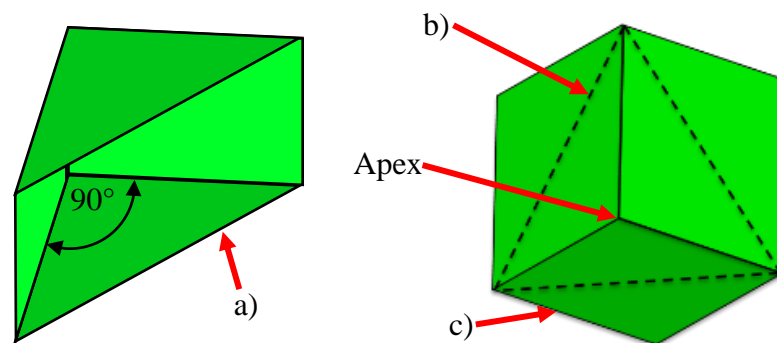
Figure 3.2 Main types of RR elements: a) RTP with rectangular aperture, b) CC with triangular aperture, and c) CC with hexagonal aperture

Traditionally, automotive manufacturers make use of plastic injection moulding to produce the majority of RR elements which are installed on modern cars (Brinksmeier *et al.*, 2008). The functionality of all RRs relies on the total internal reflection (TIR) phenomenon which essentially occurs when a ray propagating through a homogeneous/isotropic medium intersects a boundary surface at an angle larger than the critical angle (Θ_c) (Kim and Lee, 2007). Under these circumstances, the ray will be reflected back at an equal angle (Figure

3.3). For incident angles smaller than Θ_c, the ray will be refracted at an angle determined

by Snell's law (Poole, 2007). Evidently, when the incident angle is equal to Θ_c, the ray will

remain trapped into the surface delimiting the two adjacent media.
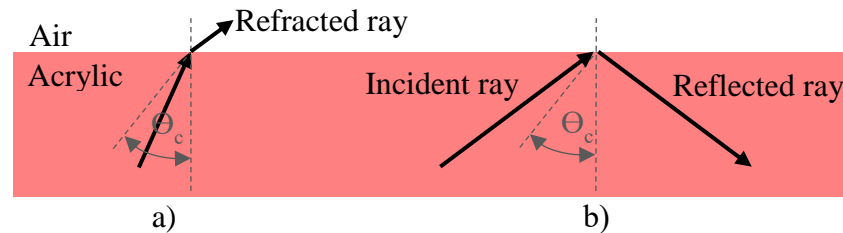
Figure 3.3 Refraction and reflection at the boundary between media: a) refraction for
incident angles $< \theta_c$, and b) TIR for incidence angles $> \theta_c$

In general terms, the geometry of the RR pose significant fabrication challenges, primarily

since the optical efficiency degrades significantly as soon as the smallest manufacturing

imperfection – regardless if related to RR geometry or facet roughness – is present. Since

rotational tools cannot be used to generate concave structures that are lacking any filleted

features automotive lighting manufacturers have to rely on standard pin-bundling

techniques to fabricate CC RRs (Van Arnam, 1978; Brinksmeier *et al.*, 2012).

In brief, these approaches make use of small pins each with a single "negative"

convex retroreflective structure (e.g., ICC) that is machined and lapped at one of the ends

of the pin (Figure 3.4). These pins are then assembled into a bundle such that one desired

concave RR structure with hexagonal aperture is created by means of three adjacent pins.

The replication of the individual CC features on a surface creates the RR array that – after

nickel or silver electroplating – will eventually form the electroform insert, which

constitutes the injection moulding master.

Single pin   Pin array
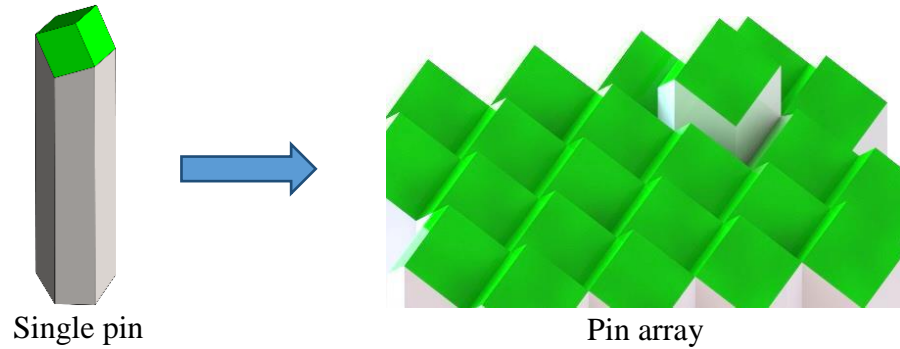
Figure 3.4 Elements of the pin-bundling technique

The miniaturization of the individual CC elements tends to enhance the optical characteristics of the overall RR array in two different ways: i) by decreasing the parallel displacement of reflected light (the distance between incident and reflected light rays), and ii) by minimizing the impact of facet distortion/imperfections on retroreflective functionality (Brinksmeier *et al.*, 2012). However, when the size/height/depth of the individual RR elements drops approximately under 500 µm, the conventional pin-bundling technique can no longer represent a viable manufacturing option, primarily because of the size and the number of pins that are to be used. The second important limitation of the conventional technique is related to the challenges that are associated with the relative positioning of the pins on curved surfaces, such as those used to define the external shape of the car.

3.4   Comparison of Optical Performance for Pin-Bundled and Machined RTP RRs

The novel RTP geometry which was recently introduced (Hussein *et al.*, 2016) will be further investigated herein in order to identify the difference in optical performance

between the RTP RRs fabricated through: i) pin-bundling, or ii) single point inverted cutting techniques (SPIC).

As outlined before, RTPs consist of a rectangular facet/aperture through which the primary beam enters and then exits, as well as two reflective facets that contribute to TIR. The parameters of a typical RTP element are shown in Figure 3.5 where W and C represent the width and the length of the aperture, respectively.
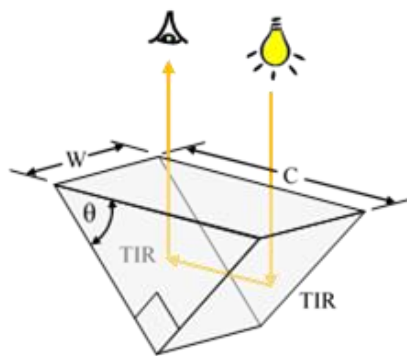
Figure 3.5 RTP geometry

As shown in the past (Hussein *et al.*, 2016), no significant differences exist between the optical performances of RTPs generated on a flat surface that is normal to the incident beam, regardless if conventional pin-bundling or newer ultraprecise SPIC were used as fabrication means.

However, the automotive industry cannot make use solely of RR elements placed on flat surfaces that are normally oriented with respect to the direction of the incident light. In fact, the majority of automotive lighting applications will require positioning of the individual RTP elements on surfaces in a different orientation with respect to the direction of the incoming rays of light.

To illustrate the differences between the RR geometries fabricated by means of the two aforementioned techniques (e.g., baseline/ conventional and SPIC), two arrays of RTP RRs were placed on a 10º inclined flat surface (Figure 3.6). As it can be noticed, when the array of RTPs is generated through cutting, no geometric discontinuities will occur between adjacent elements. However, when the array of RR elements is generated by means of the pin-bundling technique, pocket-like structures tend to appear between the neighboring RTPs, primarily due to the shape and orientation of the forming pins. These pocket-like structures represent in fact a manufacturing artifact with further implications on the optical performance of the RR array.
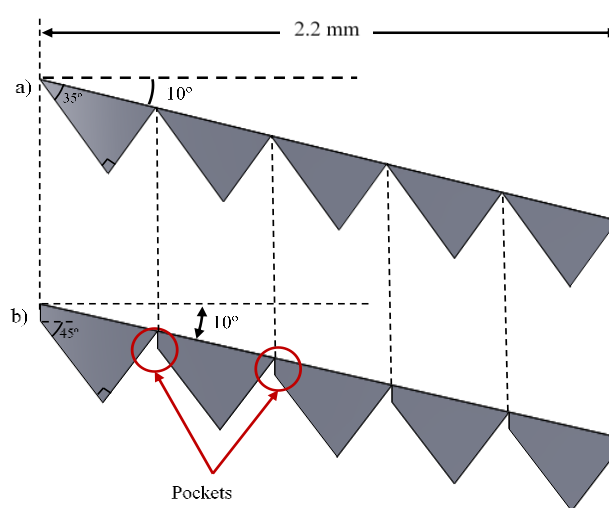
Figure 3.6 Geometry of RTP RRs fabricated on inclined flat surfaces by means of:
a) SPIC, and b) pin-bundling techniques

In order to determine the effect of the manufacturing artifacts on the optical performance, the two RTP arrays (e.g., with or without pocket-like structures) were subjected to an identical illumination setup (Figure 3.7) simulated by means of an optical simulation software.
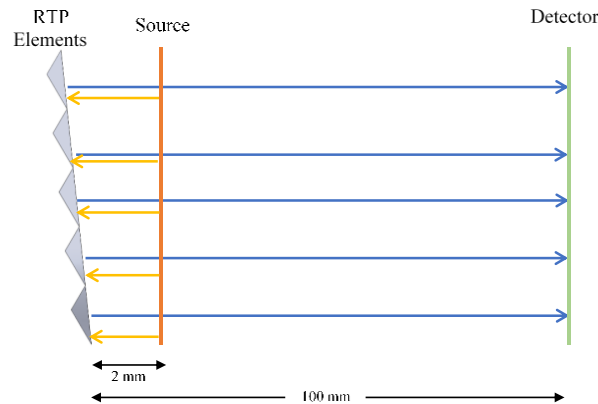
Figure 3.7 Optical simulation setup

To preserve the accuracy of the results, the two geometries were kept dimensionally comparable in a sense that each array had the same number of RR elements, characterized by identical and equal apertures (2.2 mm × 0.45 mm). As indicated above, the incident beam forms a 10º angle with the normal to the main surface on which the RR elements are to be produced. To ensure the similarity with real automotive traffic situations, the detector was intentionally placed sufficiently far from the RTP array. Along the same line of thought, the size of the detector was kept under control in order to only measure the amount of light returned to the source, where – commonly – the observer is also placed.

The general results of the optical analysis suggest that pocket-like manufacturing imperfections contribute in fact to a superior retroreflective efficiency (RRE) since 36.68% of the incident light power is returned in case of machined RTPs, while 44.54% of the incident light falls on the detector in case of RTPs produced by means of pin-bundling. The detailed trajectory of the incoming rays entering a conventionally-fabricated or cut array is presented in Figure 3.8. Here, the light originating from the source is shown in blue, and changes colour every time it intersects a medium boundary.
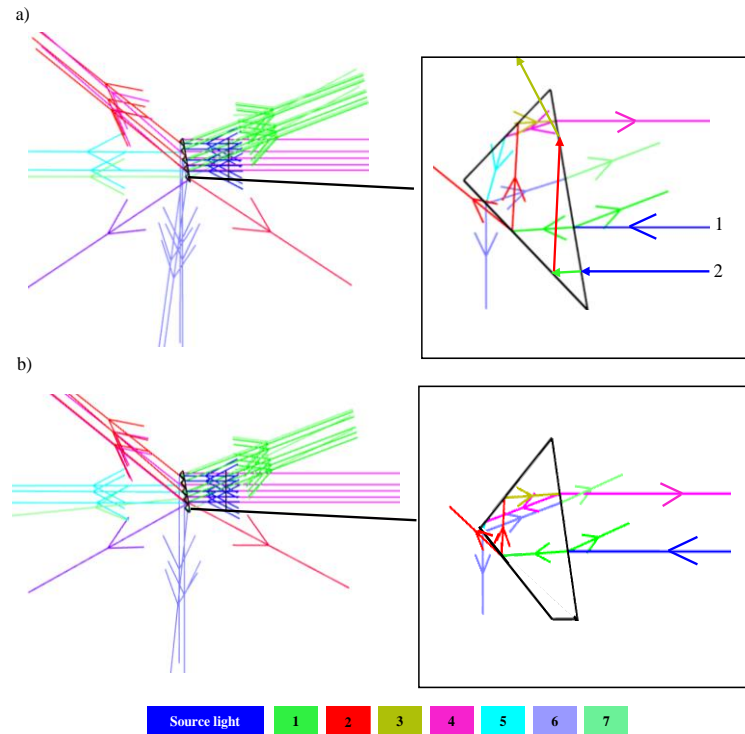
Figure 3.8 Detailed ray tracing for RTPs fabricated on the inclined flat surface through: a) inverted cutting, and b) pin-bundling

Compared to the case of maximum RRE, which occurs when the incident beam is perpendicular to the RTP incident face, the 10º tilt of the workpiece surface introduces an additional 4% loss in the form of light that is reflected but never returns to the observer/ source (green colour #1). As it can be noticed, light rays are successively reflected and/or refracted on each of the media boundary, such that the incident light ends up being spread by the RTP array in a variety of directions. While not necessarily evident, a certain amount of crosstalk exists between adjacent RTPs in a sense that a certain amount of rays are being transferred to the neighboring element after the first TIR (red colour #2). The 7.86% loss between the conventionally-fabricated RTPs and those to be produced through machining are caused by the presence of the "dead zones" that are marked by the smaller-sized arrows

in Figure 3.8a and by null irradiance in Figure 3.9 (blue coloured bands on the right side of the images). This dead zone – located at the elevated end (with respect to the incoming light direction) of the incident face of the RTP – is responsible for a decrease in the effective aperture of the optical element to be cut.

To further illustrate the presence, as well as the size, of the dead zone for the analyzed RTP arrays, Figure 3.9 outlines the correlation between the geometrical configuration of the RTP arrays and their detailed total power output. According to this analysis, while cut RTP elements are characterized by an effective aperture of 362.4 µm (Figure 3.9a), the conventionally-fabricated array yields an effective aperture of 440.0 µm (Figure 3.9b). This 17.6% difference in the effective aperture is absolutely identical to the 17.6% difference in the RRE of the two geometries and it is absolutely clear that the wider dead (e.g., blue) bands between RR elements represent its root cause.

It is important to note that although the geometrical size of the effective aperture of the conventionally-fabricated RTPs (Figure 3.9b, left) yields at 440 µm, the length of its corresponding irradiated area yields at 412.5 µm. While the cause of this discrepancy is rather unclear at this point, one possible explanation could be optical simulation errors.
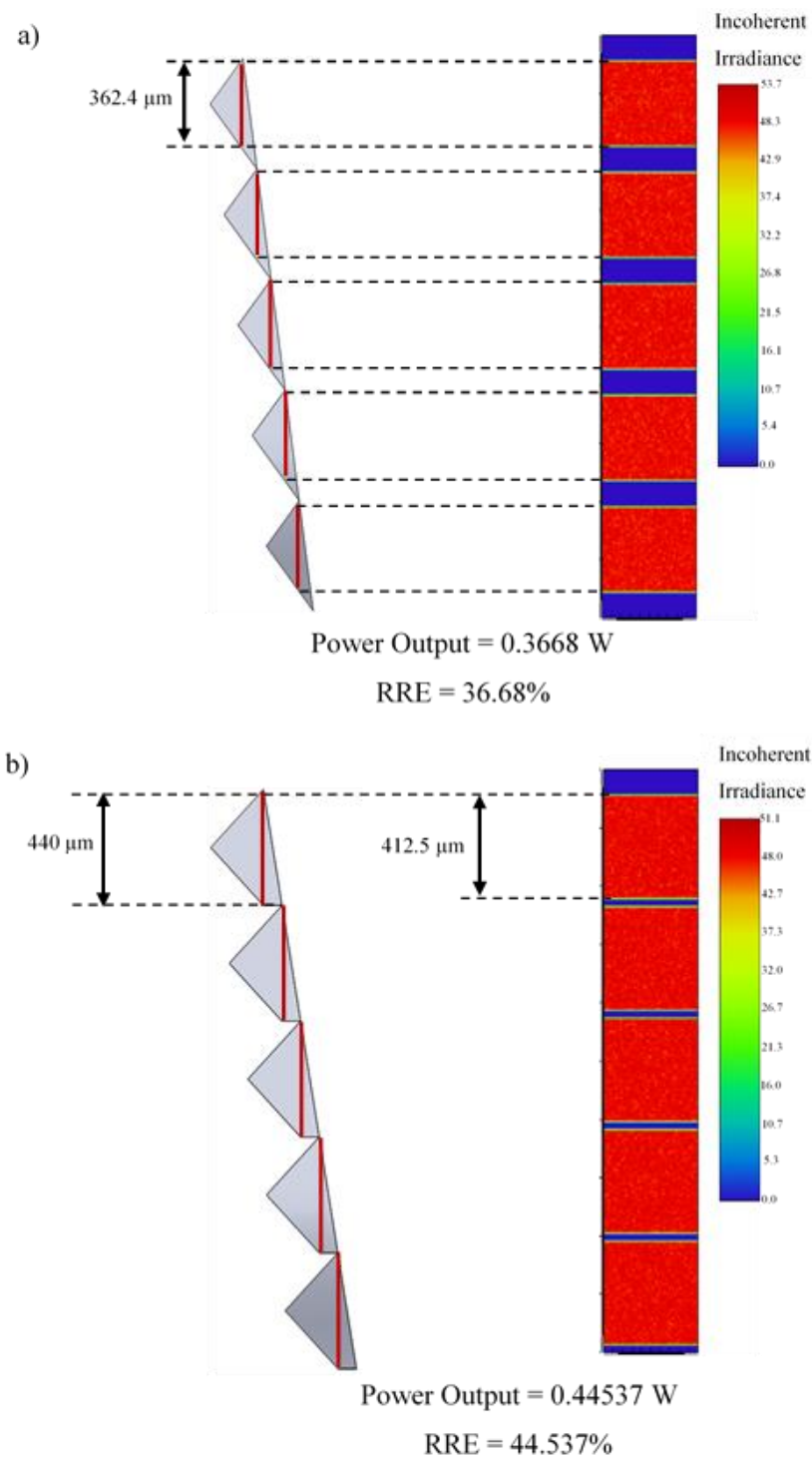
Figure 3.9 Correlation between RTP array design (grey), effective apertures (red lines) and light intensity for: a) cut RTP element, and b) conventionally fabricated RTPs

3.5 Fabrication of RTP RRs Through Ultraprecise Single Point Inverted Cutting

In order to fabricate RTP optical elements, a novel machining-based procedure has been developed. This new fabrication technique relies on a monocrystalline diamond tool that is theoretically capable to generate optical surface finishes with $R_a < 10$ nm without the need for post-machining operations. To fabricate the intended geometry, the diamond tool has to be mounted in a five-axis micromachining center capable to provide the required kinematics. Compared to the original CC retroreflectors, the geometry of the RTP can be formed easier since their apex is formed by an edge, rather than a single point. Furthermore, since RTPs are delimited by two, rather than three facets, it can be anticipated that their fabrication cycle will be proportionally shorter.

3.5.1 Ultraprecise Single Point Inverted Cutting

The development of the cutting strategies for RTP elements includes a certain degree of separation between roughing and finishing passes. Same as in the traditional machining, a roughing cut will remove more material in a shorter amount of time but will generate surfaces of lower quality and of just near-net dimensions. By contrast, finishing cuts will remove smaller amounts of material in longer amounts of time, while generating surfaces of higher quality and final size. Further considerations on both types of cuts will be introduced and examined from qualitative and quantitative perspectives.

While performing an ultraprecise single point inverted cutting operation, the diamond tool is expected to move in a short, intermittent grooving/chiseling-like motion. The primary purpose for the primary cutting motion is to ensure that the tool maintains a permanent contact with the each of the two RTP facets to be formed. For this reason, the

design of the single point inverted cutting tool replicates reasonably well that of a typical diamond turning cutter (Donaldson *et al.*, 1973; Stephenson and Agapiou, 2006), even though considerable differences exist between the short and interrupted motions that are specific to the new approach and the long and steady cuts that are specific to turning (Donaldson *et al.*, 1973).

When it comes to single point inverted cutting, machine motions can still be separated in the two traditional categories: positioning/ancillary, and cutting. In this context, a positioning move aims to align the tool with the workpiece while preparing to execute a cut. While not absolutely necessary, all five axes could become involved in the ancillary motions which can be performed at an increased speed since the tool is not engaged with workpiece material. By contrast, when cutting is performed, the direct contact between the tool and workpiece contributes directly to surface finish and tool wear (Brinksmeier *et al.*, 2012), such that it should happen at a rate appropriate for the type of material being cut.

Depending on the relative position of the tool with respect to the workpiece surface, the cutting motions involved in SPIC could be divided into two main categories, namely plunging and ploughing. More specifically, when the cutting tool is oriented in such a way that the rake angle is positive, the engagement between the tool and the workpiece could be regarded as a plunge cut. By contrast, plough cutting occurs when the rake angle is in the negative domain.

3.5.2 Monocrystalline Diamond Cutting Tool

The monocrystalline diamond tool used in SPIC shares many of its geometrical characteristics with a parting/grooving tool which is commonly used in turning. The use of the diamond insert – that is specific to ultraprecise machining – is meant to ensure an optical surface quality for the cut facets, particularly since a high surface roughness translates into a large amount of light scatter which significantly reduces the optical performance of the RTP element. This approach contrasts the conventional method in which the quality of the RR surfaces is strongly dependent on the quality of the forming end of the pins.

As depicted in Figure 3.10, the cutting geometry of the diamond insert is largely determined by three critical angles, namely: relief/clearance, wedge, and rake (Stephenson and Agapiou, 2006). According to its traditional purpose, a positive relief angle will prevent the tool from re-contacting the newly cut surface, and will thereby preserve its surface finish as yielded from the material removal operation (Stephenson and Agapiou, 2006). Depending on cutting conditions and material, relief angles typically range between 5° and 15°. A small relief angle will provide the tool with a maximum support/strength, but it – at the same time – can also lead to vibrations caused by an excessive tool contact area. Conversely, a large relief angle (generally not larger than 15°) will lead to smaller cutting forces, while reducing the overall strength of the tool tip (Stephenson and Agapiou, 2006).

α – relief angle

β – wedge angle

γ – rake angle
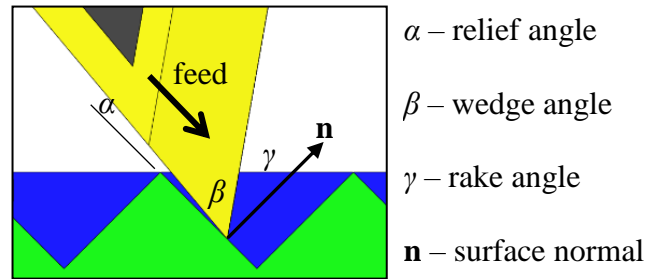
n – surface normal

Figure 3.10 Specific angles of the tool used in ultraprecise SPIC

Similar to conventional machining, the rake angle is measured between the rake face (e.g. the face of the tool in contact with chips) and the normal to the pre-machined surface which passes through the tip/cutting edge of the tool. According to general machining principles, positive rake angles will direct the chips away from the cutting interface and will thereby contribute to cutting force reductions that in turn translate in diminishes rates of tool wear (Stephenson and Agapiou, 2006; Oberg *et al.*, 2008).

The size of the third tool angle (e.g. wedge angle) is merely a consequence of the other two since their summation has to remain constant at 90°. As expected, large wedge angles will increase the tool stiffness, while smaller values will make it more susceptible to damage and/or failure under the cutting load. The final geometry of the tool fabricated for experimental trials is shown in Figure 3.11, while Figure 3.12 showcases various views of the physical tool. A wedge angle of 50° was chosen as somewhat of compromise between a cutting tool geometry that is optimized for plunging, while ensuring that plough cutting remains still possible.
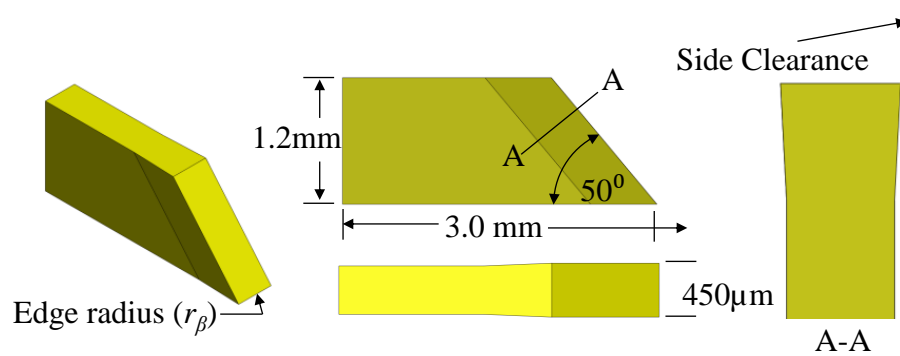
Figure 3.11 Final design of the cutting tool

Because of the orientation of the RTP geometry with respect to the tool, the relief angle during a plough cut can be no less than 90° and this in turn would result in a rake angle that is at least equal to the wedge angle. However, such cutting angles would lead to unfavorable cutting conditions, given that the use of negative rake angles should be in fact minimized. As such, this tool should be used for plunge cutting with rake angles up to 35°. According to common practice, rake angles generally range between 0 and 30°, depending on the material being cut (Oberg *et al.*, 2008).

The tool was designed with a width of 450 µm in an attempt to enable the fabrication of optical structures somewhere at the boundary between micro and macro scale. As expected, wider structures can be produced by means of successive adjacent passes (overlapping or not) generated by means of a transversal feed. However, the smallest width of the RTP structure (Figure 3.12) that can be fabricated with this tool is w = 450 µm. Note that the side (or secondary) clearance angle is meant to minimize the amount of unnecessary friction/rubbing between the tool and RTP facets that do not have an active role in TIR.
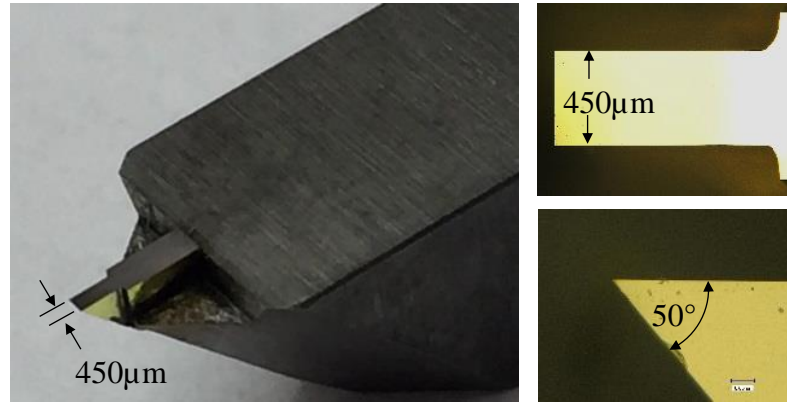
Figure 3.12 Physical cutting tool

The last dimension to be considered is the cutting edge radius (r_β). Once again, according to conventional machining knowledge, this geometric feature plays a critical role on the post-machining surface finish. More specifically, a "keen" edge (i.e., smaller cutting edge radius) would reduce the amount of cutting force and would thereby improve the overall quality of the surface. However, it is important to keep in mind that a strong tradeoff exists between the surface finish and tool wear in a sense that as cutting edge radius decreases, the tool becomes more susceptible to wear and chipping.

According to the surveyed literature, a roughing tool could have $r_\beta > 200$ nm, while finishing tools are typically expected to have $r_\beta < 60$ nm (Schönemann *et al.*, 2010). Physical experiments have shown that surface finishes could vary significantly with small changes in the cutting edge radius. However, these thresholds should be regarded as "soft", rather than "hard" limits, since their values are strongly dependent on the material being cut. More specifically, while for soft/ductile materials lower cutting edge radii translate into better surface finishes, higher values are in fact recommended for harder workpiece materials. As such, it can be inferred that the radius of the cutting edge should be large enough to increase tool life, but without doing that at the expense of a lower surface quality

which would be clearly detrimental to the optical functionality of the RR element. By taking into account all the aforementioned factors, a value of 200 nm was specified for r_β. However, the standard practice of the chosen tool supplier is to offer either a sharp or honed edge. In order to maximize the resulting surface finish, a sharp edge was chosen. The edge is inspected at $800\times$ magnification to be chip free. It is anticipated that the sharp edge will reduce the life of the tool, but this is yet to be determined.

3.5.3 Cutting Strategy

While various cutting strategies could be developed, the current study has focused on implementing one that does not require workpiece rotation/ repositioning, in an attempt to reduce the complexity of the calibration procedures involved. Because of this, three-axis motions are sufficient to fabricate the geometry of the intended RTP array. In the remainder of the section, the cutting strategy will be analyzed with an end goal to determine the length of the tool path required to cut an RTP element characterized by the following geometric characteristics: C = W = 450 µm, and $\Theta = 45°$.

An overview of the selected cutting strategy is presented in Figure 3.13. As it can be noticed, in order to avoid the need to reorient the workpiece, the two optically-functional facets of the RTP have to maintain their normals parallel with two of the translational axis of motion for the CNC machine tool. More specifically, in the selected experimental setup, the vertical facet of the RTP was positioned parallel with the XZ plane, while the horizontal facet was positioned parallel with XY principal plane of the machine tool.
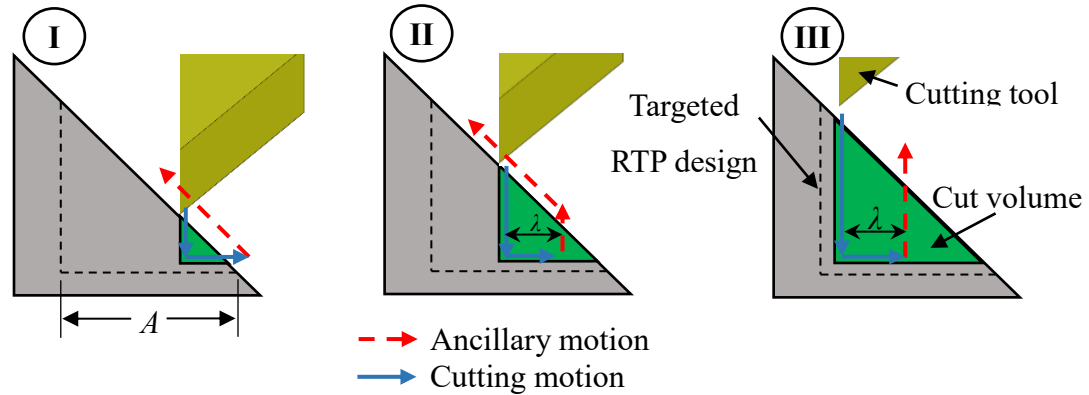
Figure 3.13 Successive sets of motions/passes in selected SPIC strategy

As it can be noticed, the cutting consists from an equal amount of plunging and ploughing instances that begin at one end of the RTP structure and then gradually advance towards the distant facet. The main role of the horizontal ploughing motion is to enable a mandatory chip breaking/separation approach. The length of the ploughing move cannot be shorter than the underformed chip thickness λ (e.g., the thickness of the new layer cut removed with each new plunging motion), since its role would be to ensure a complete/superior detachment of the chip from the RTP facet.

When the initial set of two cutting motions (e.g., vertical and horizontal or plunging and ploughing) has been completed, the tool has to be positioned at the beginning of the next set by means of two ancillary (e.g., non-cutting) motions. Since during the first auxiliary move (e.g., in the Z direction) the tool remains in contact with the workpiece at the two ends of the primary cutting edge, the triangular facets of the RTP will likely exhibit manufacturing artifacts caused by the undesirable tool contact. On the other hand, since the role of these two facets in TIR is minimal, this unwanted contact is not expected to cause any decreases in the performance of the optical element.

Based on the aforementioned considerations, the overall cutting strategy for individual RTP elements can be regarded as being comprised of a set of four consecutive motions: two for cutting purposes, and two for ancillary/tool repositioning purposes. Given the overall dimensions of the RTP element, a total of 32 different sets of motions are required to cover the length of the rectangular RTP facet a (or the cathetus of the right isosceles triangle) where: $A = C\sqrt{2}\big/2 = 318.19\,\mu m$. According to the selected cutting strategy, each of the successive cut is longer than the previous by the same length as the undeformed chip thickness, the final cut motion being 320 µm long.

3.5.4 Experimental Validation

The validation of the aforementioned cutting strategy was performed by cutting an RTP array exhibiting a brick-like pattern characterized by a C/2 (= 50%) overlap between the RTP elements positioned in adjacent rows (Figure 3.14).

a)   b)
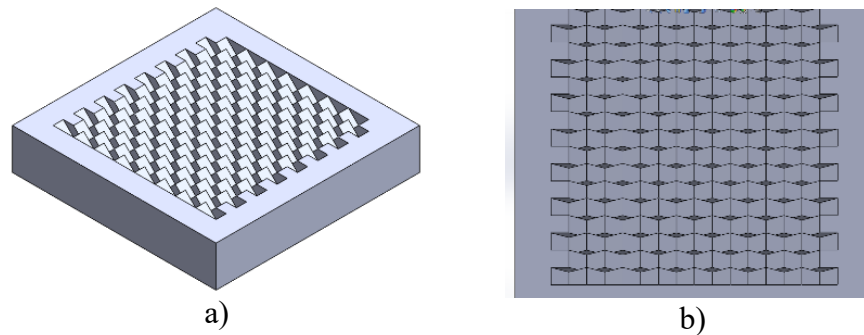
Figure 3.14 CAD model of the fabricated RTP array: a) isometric view, and b) "quasi"-top view

The array was produced on a 4 mm thick flat PMMA (e.g., polymethyl methacrylate) sheet (Figure 3.15) and was comprised of 769 RTP elements covering an area of 195 mm². Each RTP element was characterized by a square aperture of 450 × 450 µm and $\Theta = 45°$, which

is equivalent with a feature depth of 225 µm. As noticeable in SEM micrographs (Figure 3.15b), the geometry of the machined feature matches dimensionally that of its CAD counterpart.
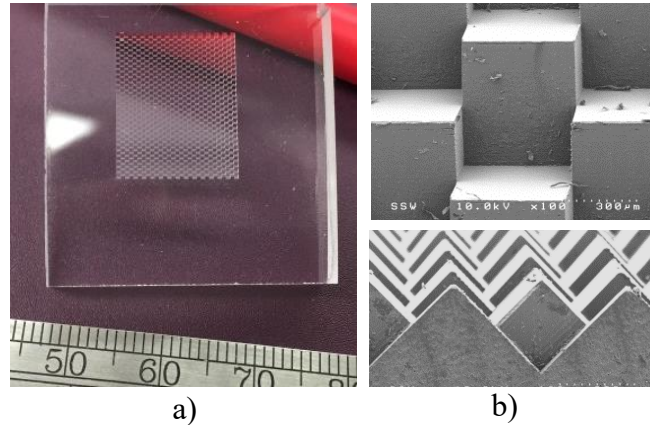
Figure 3.15 Sample workpiece: a) overview of the fabricated RTP array, and b) SEM-acquired detail views

As a drawback of the employed cutting strategy, Figure 3.16 clearly suggests that the lack of a two-phase cutting strategy (to include both roughing and finishing passes) leads to significant decreases in the roughness of the RTP facets fabricated through ploughing, rather than plunging motions.
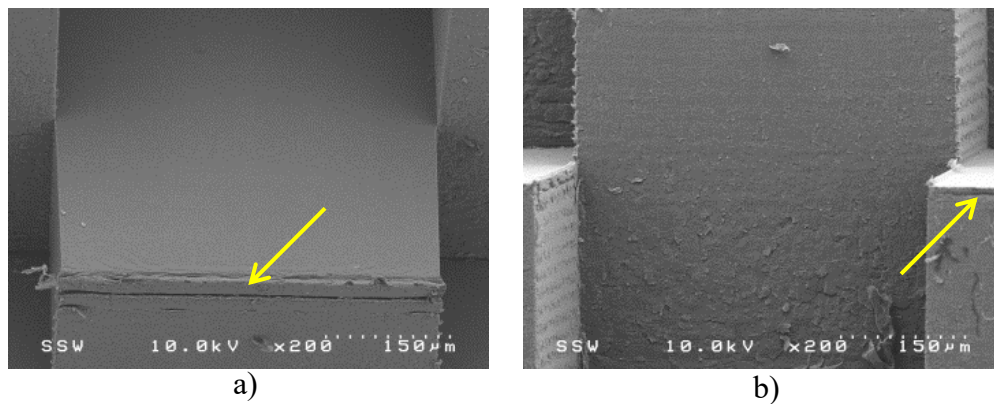
Figure 3.16 Visual appearance of the cut RTP facets obtained through: a) plunging, and b) ploughing

Moreover, certain unintentional marks, which are present at the tip of the cut RTP features (yellow arrows in Figure 3.16a/b), could be regarded as a consequence of either an incorrectly sharpened tool/chipped cutting edge or an unidentified material behavior phenomenon associated with cutting tool engagement/disengagement with the workpiece. All these issues, along with the lack of appropriate means to quantify the roughness of the cut RTP facets, will be addressed in future studies.

3.6   Assessment of the Optical Performance of the Fabricated RTP Array

The optical performance of the fabricated array was quantified by means of RRE, which can be numerically interpreted as the ratio between the retroreflected and incident light. In simple terms, an array characterized by a larger RRE will appear more luminous and this will make it more visible under low light conditions.

To perform this assessment, the fabricated array was compared directly to a conventional ICC RR used in automotive applications. As shown in Figure 3.17, both optical components were illuminated with a white LED source. While subjective to a certain extent, this preliminary testing seemed to indicate that the retroreflective array fabricated through the ultraprecise SPIC technology is more luminous than a commercial taillight that was regarded as the baseline for comparison.
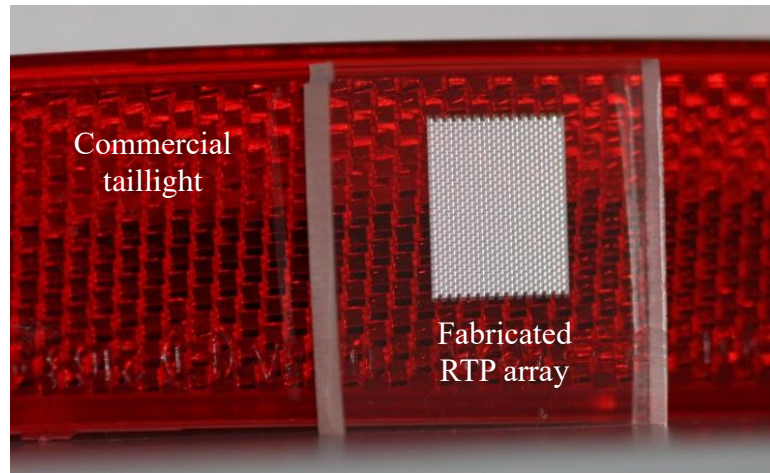
Figure 3.17 Qualitative comparison between the optical performance of the RTP array and that of a conventional ICC RR design

To quantitatively assess the difference between the optical performances of the two analyzed RR designs, the experimental setup shown in Figure 3.18 was used to measure – under darkroom conditions – the amount of the light returned to the source. The light source and the lux meter were placed adjacent to each other and 272 mm away from the retroreflectors being evaluated. Under the aforementioned experimental conditions, the light reflected by the commercial RR component was amounted to 12.6 lux, while the fabricated RTP array returned 19.8 lux.
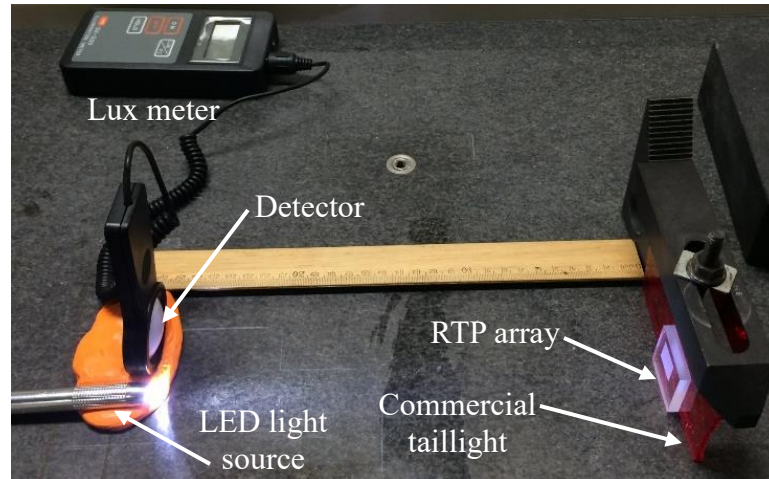
Figure 3.18 Experimental setup used in the quantitative evaluation of the optical performance

It is perhaps important to note that the 57% increase in the optical performance of the RTP array was attained even though its retroreflective area is in fact considerably smaller than that of the commercial taillight. On the other hand, it is possible that both the large flat (e.g., uncut) area surrounding the fabricated RTP arrays along with the different colour of the PMMA (i.e., white vs. red) might confound the quality of the results obtained.

3.7   Conclusions

The main objective of the present study was to introduce a new technique capable of replacing the conventional and ubiquitous pin-bundling approach in the fabrication of the RTP RR arrays, particularly since simulations performed on geometries derived from both manufacturing approaches seem to yield comparable optical performances.

The ultraprecise single point inverted cutting technique, demonstrated in the context of the present work, essentially consists of a combination of diamond turning mechanics and five-axis machining kinematics. The selected cutting strategy has demonstrated the feasibility of the newly devised fabrication technique that was able to

generate a functional RTP array prototype with an approximate area of 200 mm^2. The initial qualitative and quantitative comparisons performed between the RTP RR array prototype and a commercial taillight baseline have shown that the geometry produced through the new technique might perform better than the conventional ICC RR.

Future possible extensions of this work could be focused on: i) solving of the optical simulation inconsistencies along with the inclusion of new comparison scenarios, ii) refinements of the SPIC technology to enable a superior and measurable surface quality, and iii) enhancements to be brought to the experimental setup to be used for optical validation/assessment purposes.

3.8   Acknowledgements

3.9 References

Brinksmeier, E., Gläbe, R. & Flucke, C. 2008. Manufacturing of molds for replication of micro cube corner retroreflectors. *Production Engineering, 2*, 33–38.

Brinksmeier, E., Glabe, R. & Schonemann, L. 2012. Diamond Micro Chiseling of large-scale retroreflective arrays. *Precision Engineering-Journal of the International Societies for Precision Engineering and Nanotechnology, 36*, 650–657.

Donaldson, C., Lecain, G. & Goold, V. C. 1973. *Metal Cutting Theory and Practice,* Boca Raton, Taylor and Francis.

Hussein, S., Hamilton, B., Tutunea-Fatan, O. R. & Bordatchev, E. V. 2016. Novel Retroreflective Micro-Optical Structure for Automotive Lighting Applications. *SAE International Journal of Passenger Cars – Mechanical Systems, 9*.

Kim, H. & Lee, B. 2007. Optimal design of retroreflection corner-cube sheets by geometric optics analysis. *Optical Engineering, 46*, 094002-094002-14.

Oberg, E., Jones, F., Horton, H. & Ryffel, H. 2008. *Machinery's Handbook, 28th Edition,* New York, Industrial Press.

Poole, C. 2007. *The Physics Handbook,* Federal Republic of Germany, Wiley-VCH.

Schönemann, L., Brinksmeier, E., Flucke, C. & Glabe, R. 2010. Tool-Development for Diamond Micro Chiseling. *Uespen International Conference.* Delft.

Seward, G. H. & Cort, P. S. 1999. Measurement and characterization of angular reflectance for cube-corners and microspheres. *Optical Engineering, 38*, 164–169.

So, B. S., Jung, Y. H. & Lee, D. W. 2002. Shape design of efficient retroreflective articles. *Journal of Materials Processing Technology, 130*, 632–640.

Stephenson, D. & Agapiou, J. 2006. *Metal Cutting Theory and Practice 2nd Edition,* Boca Raton, Taylor and Francis.

Van Arnam, D. 1978. *Method for Forming Retroreflective Sheeting*. U.S. patent application 4243618. January 6, 1981.

CHAPTER 4

Fabrication of Right Triangular Prism Retroreflectors
through 3½½-Axis Ultraprecise Single Point Inverted Cutting

4.1 Overview

Retroreflectors (RR) are passive optical structures that are capable of returning incident light back to the source. The focus of the current study is represented by the right triangular prism (RTP) geometry, which could be a more efficient alternative to the traditional inverted corner cube geometry. While current manufacturing practices rely solely on the use of conventional pin-bundling techniques, the work reported in this study presents further enhancements of the previously introduced ultraprecise single point inverted cutting technique, which can be used in a manner approximately similar to 3½½-axis kinematics. The experimental results obtained have demonstrated both the feasibility of the proposed fabrication approach as well as the optical viability of the fabricated RTP elements.

Keywords: Automotive lighting, retroreflector design, optical performance, 3½½-axis diamond cutting

4.2 Introduction

A retroreflector (RR) is a passive optical device that reflects light back to the originating source through a range of incident angles deviating from the normal axis. RRs can be divided into two categories: lens-and-mirror, and inverted corner cube (ICC). As depicted in Figure 4.1a, the lens-and-mirror type, also referred to as cat's eye, are made of transparent spheres with a reflective layer on the back. The sphere has a refractive index greater than air which causes the light entering the sphere to be directed to the reflective surface. The reflected light is then refracted again as it leaves the sphere, and because of that, it ends up travelling in a direction that is parallel to the incident light (Nilsen and Lu, 2004). Alternatively, the ICC retroreflector consists of three mutually orthogonal surfaces

each contributing to retroreflection (Figure 4.1). In the case of this retroreflective element, the incident light reflects off each facet and after three successive reflections will be reflected back to the source according to a phenomenon called total internal reflection (TIR) (Seward and Cort, 1999). More details about the construction and functionality of RRs can be found in (Seward and Cort, 1999; Brinksmeier *et al.*, 2012).
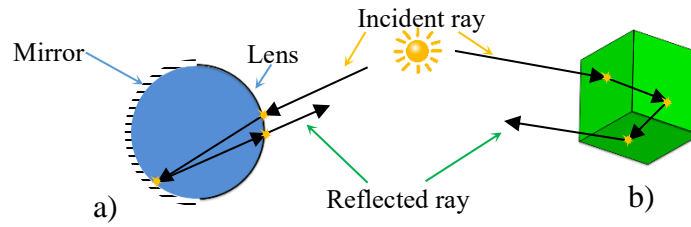
Figure 4.1 Functionality of typical RR elements: a) lens-and-mirror, and b) inverted corner cube

Retroreflective arrays have found many industrial applications, including, but not limited to traffic safety, communications, and metrology. Moreover, its superior efficiency at long distances makes the ICC appropriate for the needs of the automotive industry (Nilsen and Lu, 2004) and the typical example in this category is represented by the taillights installed on virtually all transportation vehicles (Seward and Cort, 1999).

However, the fabrication of the corner cube geometry poses an inherent challenge in a sense that rotating tools cannot be used to produce the geometry of the ICC, particularly around its apex. Because of this, the "workaround" that has been in use for several decades involves the use of the pin-bundling technique (Van Arnam, 1978). According to this method, the "negative" (*e.g.* the core) of each RR element in the array is formed by means of the end of a hexagonal pin that in turn is produced through conventional machining followed by lapping in order to attain the $R_a < 10$ nm surface finish that is required for

optical reflectivity. Once individual pins are completed, they are bundled together and a cavity insert is created at their forming end by means of electroforming.

Its inherent complexity makes pin-bundling inefficient, error-prone and difficult to use for microscale features, particularly due to the stringent surface quality requirements calling for $R_a < 10$ nm – a requirement which is typically equated with optical surface quality. For this reason, more efficient and versatile retroreflector fabrication techniques are highly desirable and two new ideas have recently emerged in this regard: i) development of cutting/machining-based fabrication techniques and ii) development of alternate RR shapes, preferably of lower geometric complexity.

In response to these challenges, a new fabrication process called ultraprecise single point inverted cutting (USPIC), along with a novel RR geometry coined as right triangular prism (RTP) have been recently developed (Hamilton *et al.*, 2016; Hussein *et al.*, 2016) as viable alternatives to pin-bundling fabrication and ICC RR design, respectively. However, while the initial experiments proved that USPIC can produce the desired RTP geometry (Hamilton *et al.*, 2016), it also became clear that the combination of plunging and ploughing motions that can be generated through the sole involvement of the translational axes of a five-axis machine is insufficient to attain the intended optical surface quality. To address this, the primary goal of the current study was to fabricate the new RTP geometry through a combination of translational and rotational motions, for which purpose the development of an USPIC postprocessor becomes essential.

4.3   Design and Optical Performance of RTP Arrays

4.3.1 Optical Characterization of the RTP Element

To ensure the retroreflective functionality of the novel RTP geometry, its geometry was modeled in CAD and then subjected to optical simulation analysis performed with a specialized software. The geometry of an RTP includes two reflective facets with role in TIR and one incident facet/aperture through which light enters and then exits (Figure 4.2). According to the automotive use of the RRs, an illumination element whose size is determined by *thickness*, *width* and *base* was joined with the incident face of the RTP.
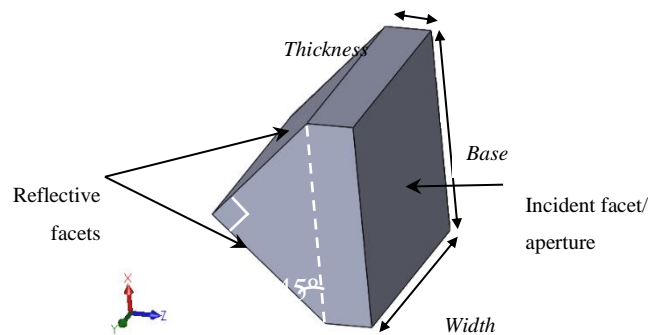
Figure 4.2 Geometry of the RTP element

To assess the optical performance of the new RTP design, the retroreflective efficiency (RRE) – defined as the percentage ratio of retroreflected light to incidence light – was determined through a series of optical simulations in which the primary variable was the direction of the incident beam (Figure 4.3). The optical simulation model (Figure 4.3a) included an RTP element with a rectangular aperture of 0.45×0.45 mm, a light source with a rectangular shape matching that of the RTP aperture, as well as a detector capable to measure the quantity of the retroreflected light. The material assumed for RTP element was polymethyl methacrylate (PMMA).
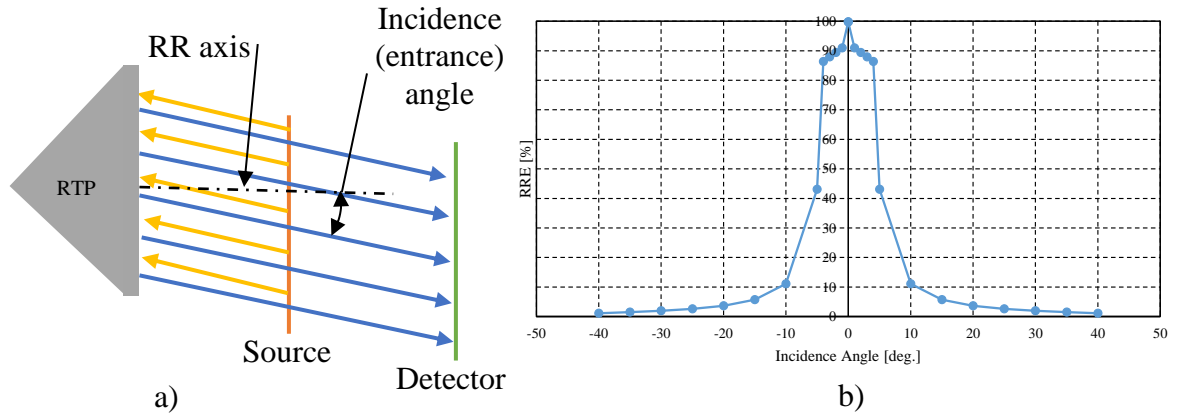
Figure 4.3 Optical performance of the RTP: a) optical simulation setup, and b) optical simulation results

The results presented in Figure 4.3b reveal that as the incidence angle increases, the RRE of the RTP element decreases since more light is lost either because it is reflected at the incident face of the illumination element or because it is never returned in the direction of the observer/detector. As such, these results imply that the best optical performance occurs when RTP's incident face is normal to the incident light. However, this theoretically "ideal" RR may not be in fact suitable for automotive lighting applications as it returns the incident light back to its source whereas this location may or may not coincide with the actual position of the observer.

4.3.2 Automatic CAD-Based Generation of the RTP array

As mentioned previously, a RR surface can be created by arranging individual RTP elements in an arrayed pattern. The base surface, in which the RTP cavities are fabricated, could have any freeform shape (*i.e.* automotive taillights), but has been assumed planar in our study to simplify the geometry. The pattern and orientation of each structure could also take on many forms, but has assumed a brick-like pattern (Figure 4.4). Geometry is

characterized by parameters which indicate the size of the array, individual element size, and how each element is positioned and oriented with respect to neighboring elements.

a) b) c)
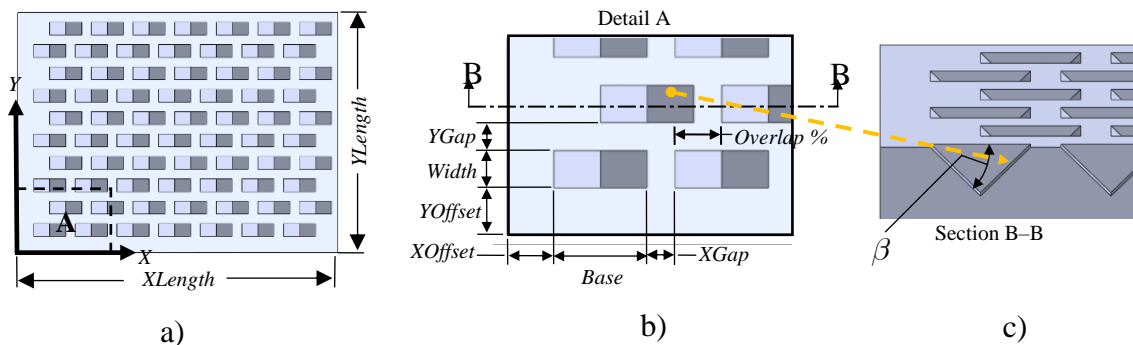
Figure 4.4 Geometrical parameters of the RTP array: a) top view of an RTP array, b) bottom left corner of the array (detail A in subfigure a), and c) cross section through RTPs (B–B plane in subfigure b)

To rapidly generate arrays belonging to the same family, a Visual Basic script/macro was created under the SolidWorks environment (Figure 4.5). The program collects all input parameters outlined in Figure 4.5 from a text file and then generates the geometry of the RTP array according to the preset design constraints and rules.
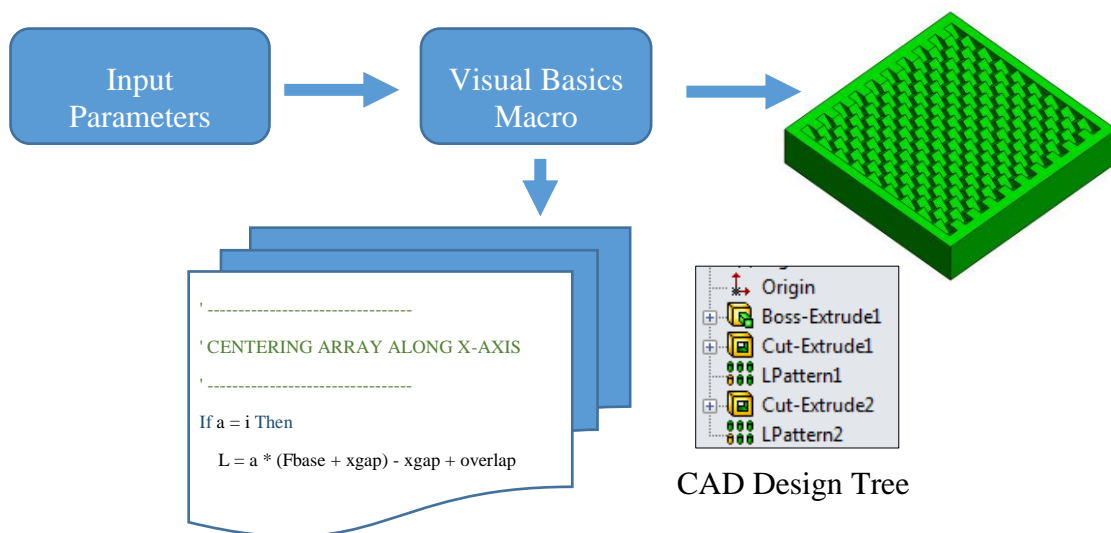
Figure 4.5 Automatic generation of the RTP array

The program first extrudes the base geometry, an operation that is followed by the calculation of the number of structures required to create the array while satisfying the input parameters. After that, the position of the first element is determined in order to ensure that the entire array is centered on the base geometry. Finally, a cut-extrude feature combined with a linear pattern is used to replicate the base RTP element in order to generate the entire array.

4.3.3 Optical Performance of the RTP Array

The procedure outlined in the section allows rapid generation of arrays with different geometric characteristics. As such, a family of RTP array geometries were investigated in an attempt to determine the correlation between their geometrical parameters and their optical performance. The two main parameters that were varied for this study were the width and the base of individual RTP elements, while all other parameters were set at constant values as follows: $XOffset = 0$ mm, $YOffset = 0$ mm, $XGap = 0$ mm, $YGap = 0$ mm, $Overlap\% = 50\%$, $XLength = 10$ mm, $YLength = 10$ mm, and $\beta = 45°$. Numerical simulation was performed on the arrays and their RRE was measured. For all optical simulations, the light was directed towards the RTP at a 0° incidence angle and all setups were absolutely identical. It can be noticed that although the RTPs covered a base flat area of identical dimensions (10 mm $\times$ 10 mm), the detector measured different RREs for different RTP sizes. This variation can be regarded as a consequence of the changes in the effective RR area defined as the total area of the reflective facets that participate in the retroreflection. The results presented in Figure 4.6 clearly indicate that with the exception of the single (e.g. non-arrayed) RTP feature covering the entire base flat surface, an inverse

proportionality relationship exists between the total effective RR area and the size/number

of arrayed RTP elements.
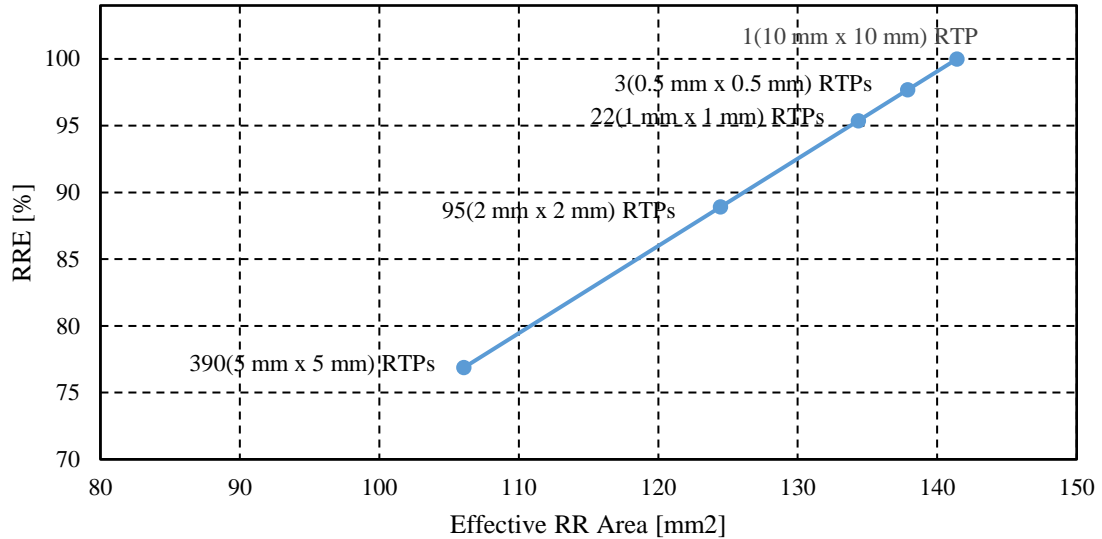
Figure 4.6 Correlation between the optical performance and the number of arrayed RTP elements

To further reiterate the dependence between array design and its associated optical

performance, the numerical values of significant optical/geometrical parameters were

summarized in Table 4.1.

Base [mm]	Width [mm]	RTPs #	Total Reflective Facets Area $[mm^2]$	Total Effective RR Area $[mm^2]$	RRE [%]
10	10	1	141.42	141.42	99.99
5	5	3	141.42	106.07	76.88
2	2	22	141.42	124.45	88.90
1	1	95	141.42	134.35	95.37
0.5	0.5	390	141.42	137.88	97.68

Table 4.1 Summary of geometrical and optical characteristics of the RTP array

To further explain this behavior, Figure 4.7 depicts two representative cases of RTP array

design along with the distribution of the reflected light as recorded by the detector. As it

can be noticed, while absolutely no loss of light exists in the case of a single RTP (Figure 4.7a), certain "dead spots" (*e.g.* non-retroreflective facets/RTPs) will exist in the case of arrayed RTPs (Figure 4.7d), particularly for the elements located on the boundary of the base surface. As the summated area of the "dead spots" decreases with the size of the elementary RTP, it becomes clear that this will translate into corresponding retroreflectivity increases. Given that the *Overlap%* parameter (Figure 4.4) was assumed at 50%, it is inevitable that some of the RTP facets will fall outside of the base 10×10 mm area.
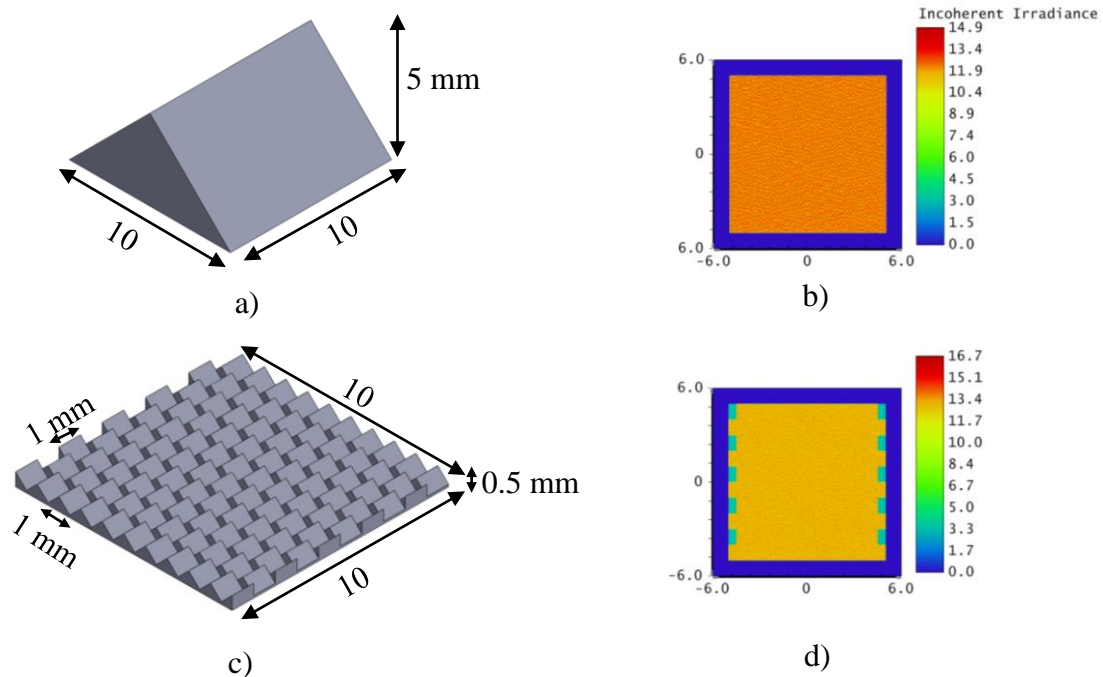
Figure 4.7 Optical performance of the RTP arrays: a) single RTP design, b) retroreflected light distribution for the analyzed single RTP, c) design of an RTP array, and d) retroreflected light distribution for the analyzed RTPs array

Based on the considerations above, it becomes apparent that while the absolute best scenario from an optical perspective would be a singular RTP instance, this would be in fact unfeasible for manufacturing/applicability reasons. Because of this, a more practical

suggestion would be to decrease the size of the RTP as much as possible, one inherent limitation being the width of the cutting tool to be used for RTP array fabrication.

4.4 Fabrication of the RTP Array through 3½⁄2½-Axis Machining

4.4.1 Diamond Cutting Tool

To fabricate the intended RTP array, a custom tool was developed and manufactured for use in USPIC operations. The cutter consists of a steel shank and a diamond tip and shares many design characteristics with cutting tools used in parting or turning operations, the primary difference being that clearance and rake faces were positioned in a rather reversed manner (Figure 4.8). The use of a diamond tip – that is specific to ultraprecise machining operations – is meant to ensure an optical quality on the retroreflective facets of the RTP (Schönemann *et al.*, 2010). If the surface finish is below the optical quality, the reflective facets will tend to scatter light and this will decrease the reflective efficiency of the elementary RTP and implicitly that of the array. In this context, it is perhaps worth to mention that while in the traditional pin-bundling-based technique the surface finish is primarily determined by the lapping operation applied on the forming end of the hexagonal pin, the quality of RTP facets is mainly dependent on the overall tool-workpiece interaction/dynamics during USPIC.
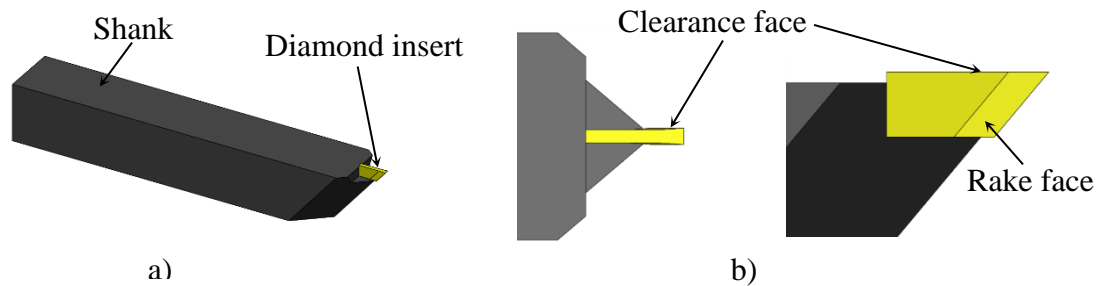
Figure 4.8 Design of the diamond cutting tool: a) overview of the cutting tool, and b) constructive detail of the tool tip

In this regard, since USPIC mechanics is somewhat similar to that of turning, the design of the USPIC tool has to adhere to comparable guidelines. As shown in Figure 4.9, three angles are critical for the entire cutting geometry: relief/clearance, wedge, and rake.

The relief angle is formed between the post-machined surface of the workpiece and the clearance face of the tool. Its presence is meant to reduce/eliminate the risk of post-machining surface damage (Stephenson and Agapiou, 2006). Typical relief angles range from 5° to 15° depending on cutting conditions, tool material, and workpiece material. On the other hand, the rake angle is measured between a normal to the post-machined surface that passed through the tool tip and the rake face of the tool. According to conventional machining theory, the rake angle determines how the chip develops during the cutting process in a sense that a positive angle (Figure 4.9) is associated with decreased cutting forces leading to an improved tool life (Stephenson and Agapiou, 2006; Oberg *et al.*, 2008). Since rake angle values are largely determined by the material being cut, values between 0º and 30º are typically recommended (Oberg *et al.*, 2008; Brinksmeier *et al.*, 2012). Finally, the wedge angle is determined as the 90º complement of rake and relief angles

($\alpha + \beta + \gamma = 90°$). As such, a large wedge angle (*i.e.* close to 90°) is associated with a stiff tool, while a smaller wedge angle makes the cutter more susceptible to failure.

α – relief angle

β – wedge angle

γ – rake angle

n – surface normal
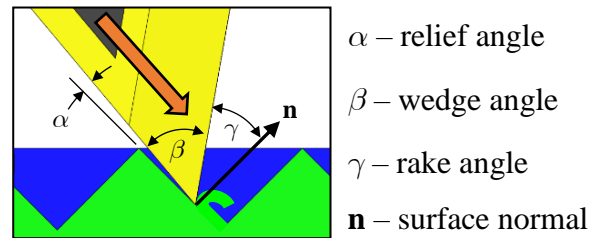
Figure 4.9 Cutting geometry and tool angles

Similar to turning, the radius of the cutting edge (r_β) has a strong effect on the surface finish as well as the durability of the tool (Schönemann *et al.*, 2010). The tool used in RTP cutting operations is characterized by a 50° degree wedge angle which in turn enables a wide range of rake and clearance angles. Based on the considerations presented in Section 2.2, the tool was fabricated with a width of 1 mm in an attempt to maintain the RTP structures dimensionally comparable to their ICC equivalents that are commonly used in automotive lighting applications. To minimize the presence of "dead" (*e.g.* unreflective) zones of the RTP facets around the apex, the radius of the cutting edge was reduced to the minimum attainable value ($r_\beta \approx 0$).

4.4.2 Cutting Motions and Strategies

When it comes to the fabrication of an RTP array, different cutting strategies can be imagined. The "unidirectional" strategy that was previously (Hamilton *et al.*, 2016) introduced for individual RTPs consists of a combination of plunging and ploughing motions. The primary difference between the two main types of motions consists in the relative position between the tool and the workpiece (Figure 4.10). Evidently, while the large positive rake angle associated with the plunging motion facilitates chips evacuation,

its negative value – characteristic to a ploughing cut – will translate into a decreased quality on the corresponding RTP facet. Furthermore, the increased cutting forces make the cutter more susceptible to failure during ploughing.
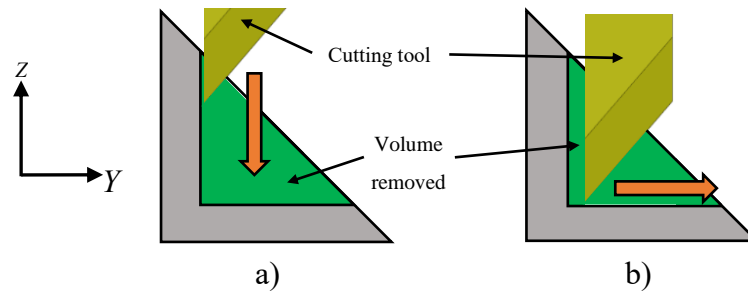
Figure 4.10 Principal motions in unidirectional RTP cutting: a) plunging, and b) ploughing

Figure 4.10b suggests that in order to achieve ideal cutting conditions on the second RTP facet, the tool should be in fact rotated in a counterclockwise direction by 90°. However, this position is geometrically unfeasible, such that other cutting strategies have to be used in order to overcome the aforementioned drawbacks of the ploughing motion, possibly by involving plunging motions only. On the other hand, the main advantage of this unidirectional approach resides in the fact that repositioning (through rotation) of the workpiece is not necessary, such that three-axis kinematics was sufficient to generate the intended RTP array geometry.

To further improve the roughness of both facets of the RTP, a novel cutting strategy was developed in the context of the current study. According to this new technique, the cutting starts by roughing out the cavity of the RTP element in a unidirectional manner similar to the one depicted in Figure 4.11. It is important to note that – if the RTPs are to cut on a base flat surface, the workpiece should be held in a rotated ($A = 45º$). With the exception of a small portion at the beginning of the cut, roughing consists of a four-step

sequence comprised of two cutting and two ancillary motions required to position the tool for the next cutting cycle. During roughing, the horizontal cutting motion has to exceed the thickness of the layer being cut (λ) in order to ensure a successful chip separation. Evidently, the length of the cutting increases as the roughing progresses.
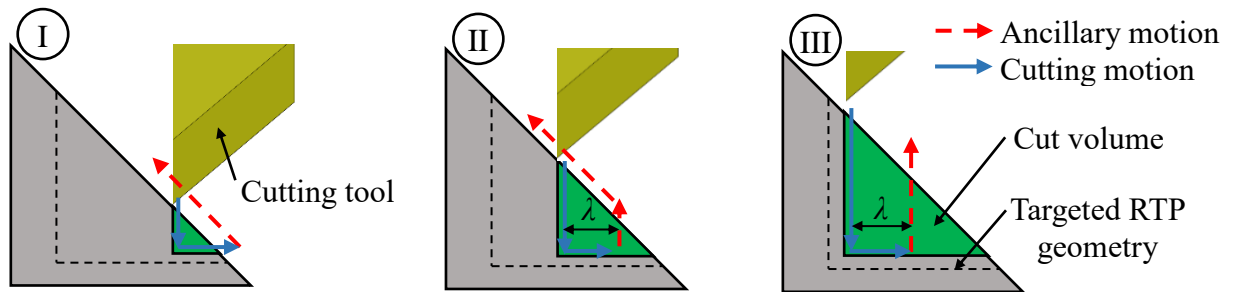
Figure 4.11 Roughing sequence

Once the near-net shape of the RTP is achieved, a cut performed solely by means of plunging was used to finish the facet that has was previously subjected to ploughing only. In order to implement the finish strategy, an appropriate machine tool setup and/or calibration was critical in obtaining the intended optical surface quality (Brinksmeier *et al.*, 2012). For this purpose, the tool was installed by ensuring the parallelism between the clearance face and the XZ plane of the multi-axis machine tool. Since similar strict parallelism conditions were also enforced between the cutting edge and the X-axis of the machine, an adjustable cutting tool fixture was designed and used for this purpose. In order to orient the horizontal facet – that was roughed out through ploughing – in a vertical position, workpiece rotation is mandatory, such that a five-axis machine tool with rotary table configuration was employed for this purpose (Figure 4.12). However, since the rotational axes have merely a positioning/indexing role, the proposed strategy resembles a traditional 3½½-axis machining operation that is also sometimes termed as 3+2, inclined, fixed, or tilted machining (Suh and Lee, 1998; Chen *et al.*, 2003; Albert, 2006). The

addition of the rotary axes necessitates the development of a complete kinematic model of the five-axis machine tool. Its development constitutes a routine analysis in the broader context of five-axis machining postprocessors, especially since generalized kinematic models have also been proposed (Tutunea-Fatan and Feng, 2004; She and Chang, 2007).
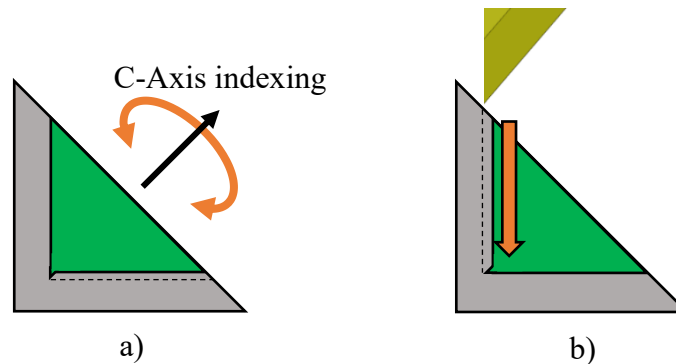
Figure 4.12 Finishing sequence performed on a roughed-out RTP: a) indexing motion, and b) finishing cut

4.4.3 Machine Tool Kinematics

In general terms, a five-axis machine tool provides additional manufacturing flexibility through the addition of two rotational degrees of freedom that supplement the three translational degrees that are offered by a classical three-axis machine. According to the terminology introduced in (Tutunea-Fatan and Feng, 2004), an *AC* rotary table five-axis micro-machine was used to demonstrate the newly-developed 3½½-axis cutting strategy. Similar to prior naming conventions, *A* represents the primary, while *C* is the secondary rotary axis.
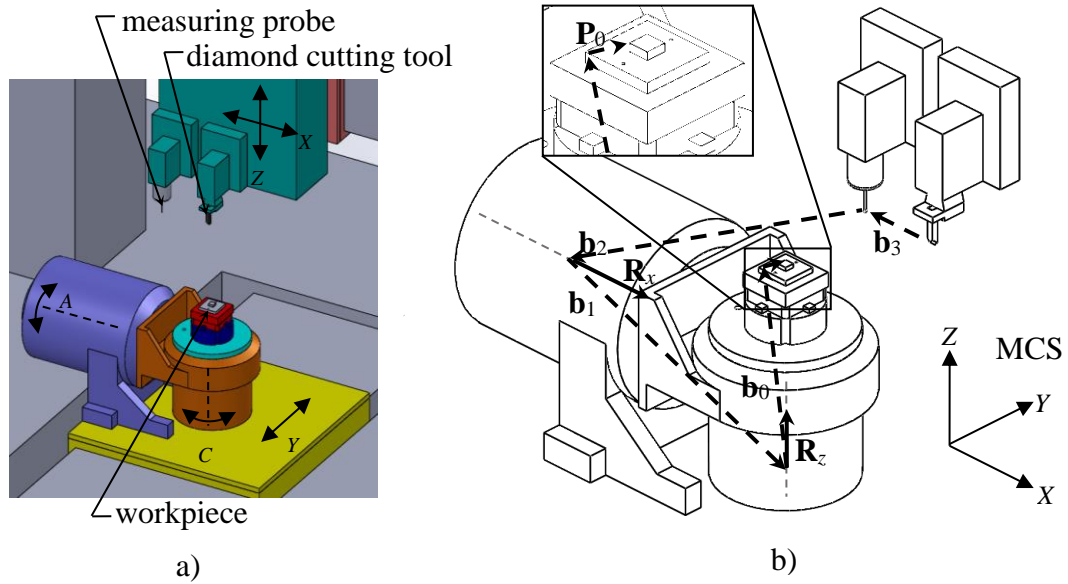
Figure 4.13 Five-axis micro-machine: a) motions, and b) inverse kinematics model

According to the robotics theory, an inverse kinematics transformation is required in order to convert the position $\mathbf{P}^W$ of the cutting point from the workpiece coordinate system (WCS) into a point $\mathbf{P}^M$ located in the machine coordinate system (MCS):

$$\mathbf{P}^M = {}_{W}^{M}\mathbf{T} \cdot \mathbf{P}^W \qquad (4.1)$$

where ${}_{W}^{M}[\mathbf{T}]$ represents the generalized coordinate transformation matrix from WCS to MCS (Tutunea-Fatan and Feng, 2004).

As illustrated in Figure 4.13, each joint connects different links of the kinematic chain (Tutunea-Fatan and Feng, 2004; Boz and Lazoglu, 2013), and in turn each of the joints is associated with one of the five degrees of freedom. The relative position between successive joints is determined by the positional matrices $\mathbf{b}_i$, while the relative orientation between them is quantified by means of the rotational matrices $\mathbf{R}_i$. As such, the kinematic chain depicted in Figure 4.13 can be described by means of four position vectors (*e.g.* $\mathbf{b}_0$,

$\mathbf{b}_1$, $\mathbf{b}_2$, and $\mathbf{b}_3$), and two rotational matrices (*e.g.* $\mathbf{R}_X$ and $\mathbf{R}_Z$). In general terms, $\mathbf{b}_i$ can be described as:

$$\mathbf{b}_i = \begin{bmatrix} 1 & 0 & 0 & x_i \\ 0 & 1 & 0 & y_i \\ 0 & 0 & 1 & z_i \\ 0 & 0 & 0 & 1 \end{bmatrix} \tag{4.2}$$

while the general rotation matrix $\mathbf{R}_i$ about an arbitrary vector in space $\mathbf{n}^t = \begin{bmatrix} n_x & n_y & n_z \end{bmatrix}$ is (Zeid, 2005):

$$\mathbf{R}_i = \begin{bmatrix} n_{x_i}^2 v\theta + c\theta & n_{x_i} n_{y_i} v\theta - n_{z_i} s\theta & n_{x_i} n_{z_i} v\theta + n_{y_i} s\theta & 0 \\ n_{x_i} n_{y_i} v\theta + n_{z_i} s\theta & n_{y_i}^2 v\theta + c\theta & n_{y_i} n_{z_i} v\theta - n_{x_i} s\theta & 0 \\ n_{x_i} n_{z_i} v\theta - n_{y_i} s\theta & n_{y_i} n_{z_i} v\theta + n_{x_i} s\theta & n_{z_i}^2 v\theta + c\theta & 0 \\ 0 & 0 & 0 & 1 \end{bmatrix} \tag{4.3}$$

For both Equations. 4.2 and 4.3, i is the index of the joint, θ is the rotational angle around the $\mathbf{n}_i$ vector, while the other expressions are simplified trigonometric forms: $c\theta = \cos\theta$, $s\theta = \sin\theta$, $v\theta = 1 - \cos\theta$.

It is important to emphasize here that while rotational matrices can be reduced to much simpler expressions, the inherent precision required for the RTP fabrication operation requires a careful account of the misalignments that are present along the kinematic chain. In line with this thought, after the completion of the calibration routines, it was found that the actual cosine directors of the two rotational axes of the machine were:

$$\delta\mathbf{n}_{\mathbf{R}_X}^{\ t} = \begin{bmatrix} 0.999995 & -0.0014502 & 0.00268292 \end{bmatrix} \tag{4.4}$$

and

$$\delta \mathbf{n}_{\mathbf{R}_Z}{}^t = \begin{bmatrix} -0.00015666 & 0.00048007 & 0.99999987 \end{bmatrix} \qquad (4.5)$$

which are close, but not coincident with their theoretical values, *i.e.* $\begin{bmatrix} 1 & 0 & 0 \end{bmatrix}$ and $\begin{bmatrix} 0 & 0 & 1 \end{bmatrix}$, respectively.

Based on all the above considerations, a more detailed form of the generalized coordinate transformation matrix used in Equation (4.1) can be written as:

$$_W^M\mathbf{T} = \mathbf{b}_3 \cdot \mathbf{b}_2 \cdot \mathbf{R}_X \cdot \mathbf{b}_1 \cdot \mathbf{R}_Z \cdot \mathbf{b}_0 \qquad (4.6)$$

which constitutes in fact the core of the required inverse kinematics transformation.

4.5   Experimental Validation

To test the proposed fabrication approach, several RTP features were machined on a top flat face of a PMMA block (Figure 4.14a, and Figure 4.14b). The feed rates used for roughing and finishing varied between 100 mm/min and 10 mm/min, while the corresponding layer thicknesses were selected at 10 µm and 1 µm, respectively. Since the primary goal of the experimental validation was to assess the quality of the fabricated RTP elements (Figure 4.14c, and Figure 4.14d), no enlarged arrays were generated at this time. Instead, the majority of the RTPs were located in positions that can be placed at the appropriate focal distance for the optical profilometer used for surface roughness evaluation (Figure 4.14d).
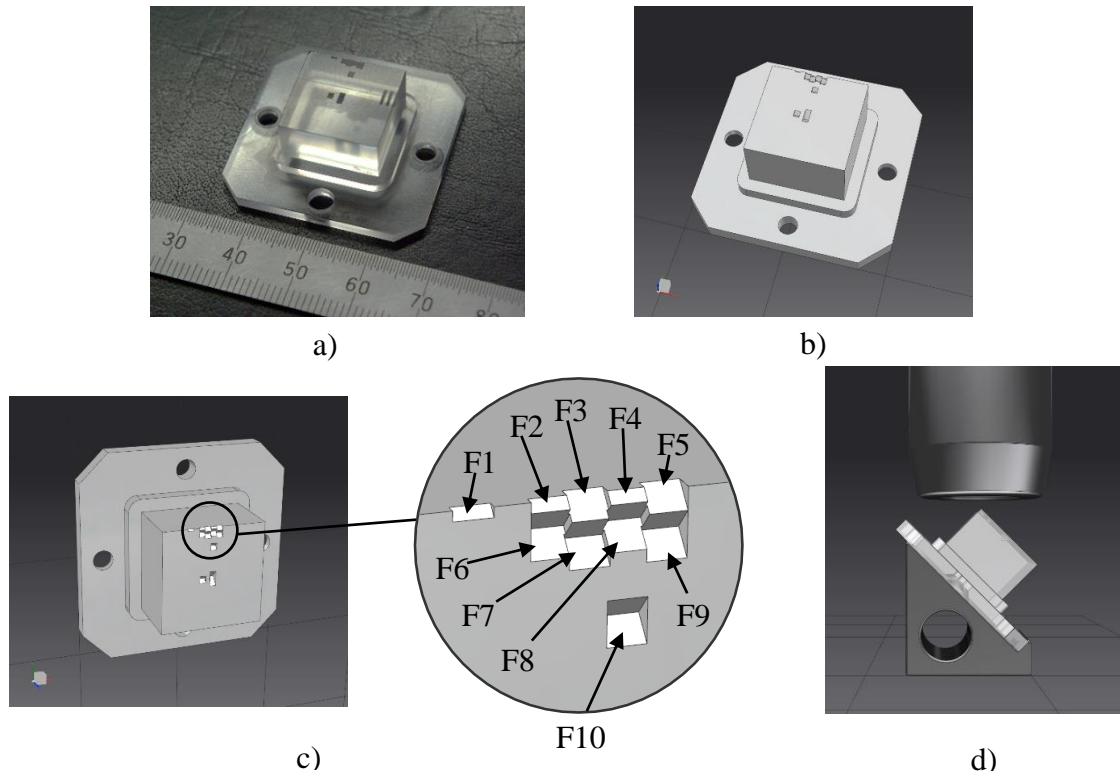
Figure 4.14 RTP elements generated for validation purposes: a) physical test workpiece, b) CAD-rendered workpiece, c) facet labeling for roughness assessment, and d) relative positioning between the workpiece and microscope objective

A summary of the surface quality results obtained during trials is presented in Table 4.2 Quality of the fabricated RTP facets. According to these values, $S_a = 147.07 \pm 41.37$ nm for all 10 assessed facets.

Facet	Average Areal Surface Roughness S_a [nm]	Facet	Average Areal Surface Roughness S_a [nm]
F1	191.28	F6	121.63
F2	190.36	F7	90.19
F3	109.21	F8	114.40
F4	179.54	F9	114.46
F5	201.36	F10	158.26

Table 4.2 Quality of the fabricated RTP facets

A more in-depth analysis of the surface quality reveals significant differences between the original unidirectional approach (Figure 4.15) and the proposed 3½½-axis cutting technique (Figure 4.16). As a general comment, the quality of the facets obtained through plunging seems to be more than 4 times better than that obtained through ploughing. Beyond that, even if the cutting process seems to be somewhat difficult to stabilize at this time (90.19 nm $\leq S_a \leq$ 191.28 nm), its quality can be brought close to the optical quality (Figure 4.16c).
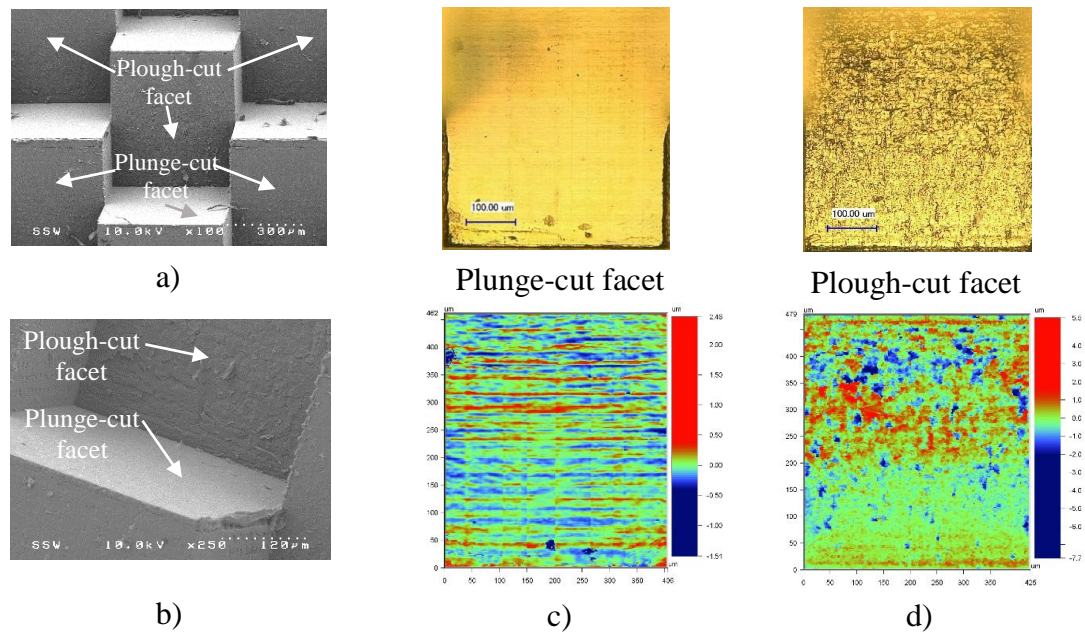
Figure 4.15 Uni-directional cutting quality: a) broad-field SEM micrograph, b) close-up SEM micrograph, c) optical (top) and topographic (bottom) images of the plunge-cut facet (S_a = 114.55 nm), and d) optical (top) and topographic (bottom) images of the plough-cut facet (S_a = 468.19 nm)
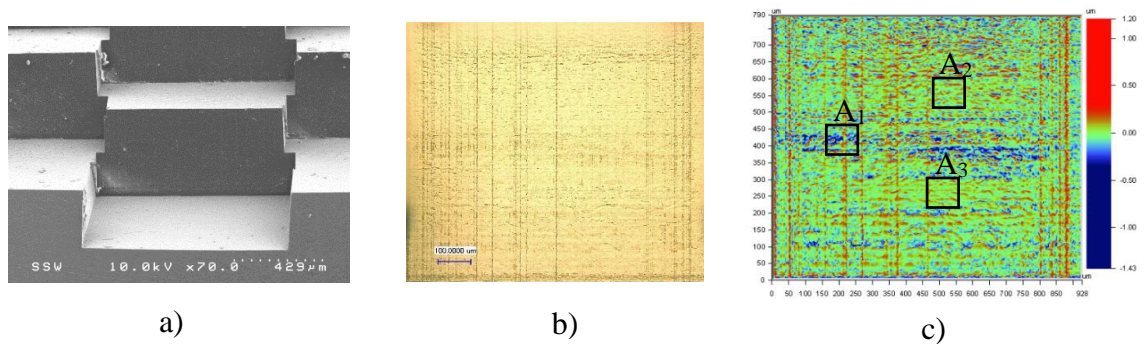
Figure 4.16 Quality of 3½½½-axis cutting: a) broad-field SEM micrograph, b) optical image of facet F7 ($S_a = 90.19$ nm), and c) topographic image of facet F7 ($S_{a_{A_1}} = 120.23\,\text{nm}, S_{a_{A_2}} = 70.56\,\text{nm}, S_{a_{A_3}} = 50.63\,\text{nm}$)

One of the largest contributors to the significant decreases in surface quality was represented by the occurrence/development of chips on the cutting edge that in turn have translated into veritable scratches/grooves on the surface of the RTP facets (Figure 4.17) While the rationale behind their formation remains at this time unclear, it is possible that they have appeared due to a combination of incorrectly sharpened tool edge and/or workpiece material build-up. The size of the chips/scratches varies, but the majority of them remain below 5 μm wide while their length stretches over the entire RTP facet.
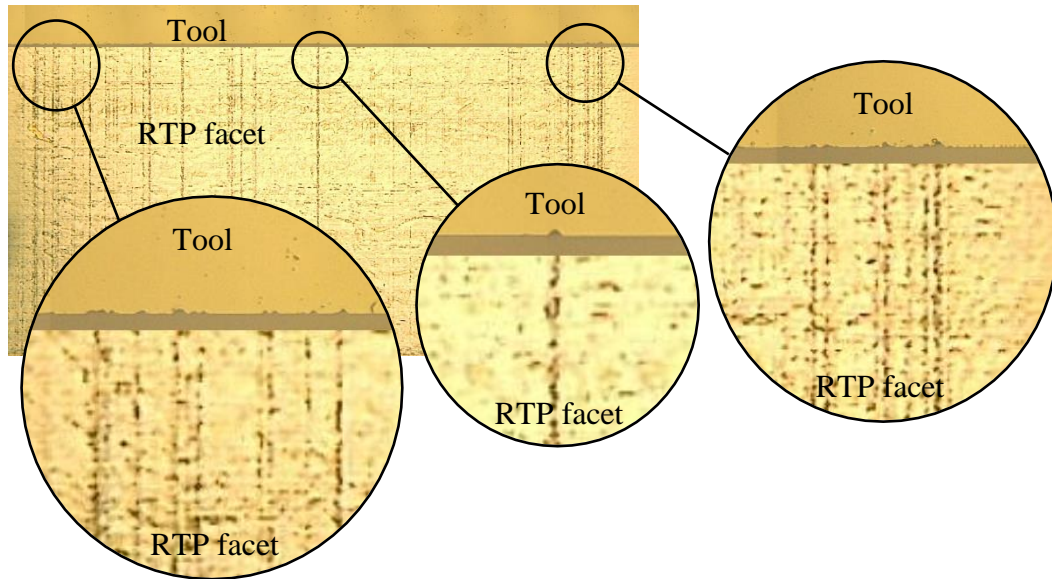
Figure 4.17 RTP facet scratches caused by chipping of the diamond tool cutting edge.

As a final verification of their optical functionality, the fabricated RTP elements were subjected to an incident light that was projected from the back of the workpiece (Figure 4.18). This setup mimics the real working scenario in which the RTPs will be used, as the machined facets constitute in fact the "negative" (*e.g.* mould insert) of the final optical element. While it is true that this rather simplistic experiment can only provide a certain level of qualitative evaluation of the RTPs – at this time – it was considered that this is sufficient to demonstrate that the proposed technique can generate functional optical elements that are visible under a wide incidence angle – a desirable trait in safety applications.
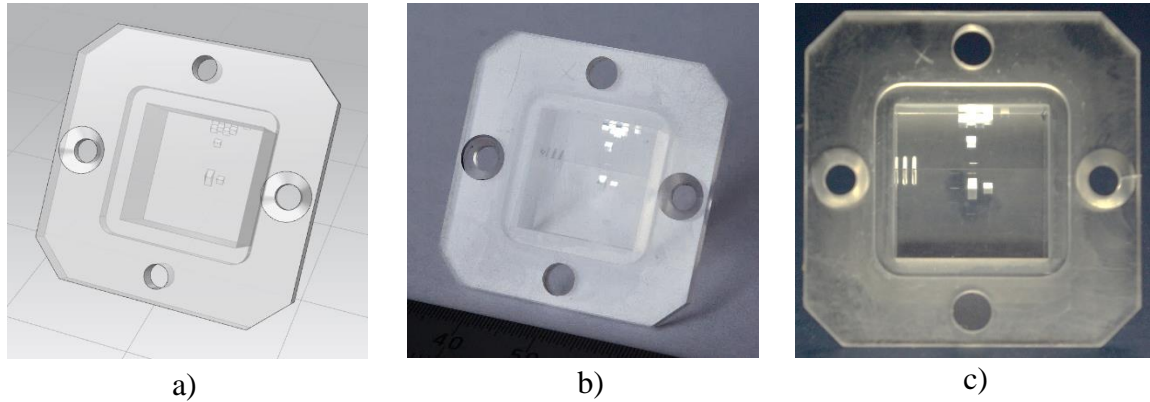
Figure 4.18 Optical functionality of the fabricated RTP: a) CAD-rendered image of the workpiece, b) lateral illumination, and c) normal-to-aperture illumination.

4.6   Conclusions

The primary objective of this study was to further enhance the unidirectional cutting technique that was previously proposed for fabrication of the RTPs. Since the only way to further improve the quality of the RTP facets is by producing them exclusively by means of plunge-cutting, a new 3½½-axis USPIC technique was developed for this purpose.

However, prior to being considered for fabrication, an automatic CAD-based procedure was devised to quickly generate parametrized RTP arrays that were then subjected to optical simulations in order to determine an optically-performant size for them. Following this, an inverse kinematics model of the five-axis machine used during cutting experiments was developed and its numerical parameters were adjusted according to the data collected through calibration experiments. The experiments performed revealed that the proposed 3½½-axis cutting technique can generate RTP facets with average areal roughness around 150 nm that in some cases can be as low as 50 nm. The RTP elements that were produced by means of the new approach proved to be optically functional.

In summary, the proposed 3½½½-axis USPIC technique has proved to be a viable fabrication option for the RTP elements. Future work will attempt to improve further the quality of the retroreflective facets, as well as to improve the productivity of the overall manufacturing process.

4.7   Acknowledgements

4.8   References

Albert, M. 2006. An Overview of 3+2 Machining. *Modern Machine Shop.*

Boz, Y. & Lazoglu, I. 2013. A postprocessor for table-tilting type five-axis machine tool based on generalized kinematics with variable feedrate implementation. *International Journal of Advanced Manufacturing Technology,* **66**, 1285–1293.

Brinksmeier, E., Glabe, R. & Schonemann, L. 2012. Diamond Micro Chiseling of large-scale retroreflective arrays. *Precision Engineering-Journal of the International Societies for Precision Engineering and Nanotechnology,* **36**, 650–657.

Chen, Z. Z. C., Dong, Z. M. & Vickers, G. W. 2003. Automated surface subdivision and tool path generation for 3 1/2 1/2-axis CNC machining of sculptured parts. *Computers in Industry,* **50**, 319–331.

Hamilton, B., Hussein, S., Tutunea-Fatan, O. R. & Bordatchev, E. V. 2016. Fabrication of Right Triangular Prism Retroreflectors through Ultraprecise Single Point Inverted Cutting. *Manufacturing Science and Engineering Conference.* Blacksburg, Virginia.

Hussein, S., Hamilton, B., Tutunea-Fatan, O. R. & Bordatchev, E. V. 2016. Novel Retroreflective Micro-Optical Structure for Automotive Lighting Applications. *SAE International Journal of Passenger Cars – Mechanical Systems,* **9**.

Nilsen, R. B. & Lu, X. J. 2004. Retroreflection technology. *Optics and Photonics for Counterterrorism and Crime Fighting,* **5616**, 47–60.

Oberg, E., Jones, F., Horton, H. & Ryffel, H. 2008. *Machinery's Handbook, 28th Edition,* New York, Industrial Press.

Schönemann, L., Brinksmeier, E., Flucke, C. & Glabe, R. 2010. Tool-Development for Diamond Micro Chiseling. *Uespen International Conference.* Delft.

Seward, G. H. & Cort, P. S. 1999. Measurement and characterization of angular reflectance for cube-corners and microspheres. *Optical Engineering,* **38**, 164–169.

She, C. H. & Chang, C. C. 2007. Design of a generic five-axis postprocessor based on generalized kinematics model of machine tool. *International Journal of Machine Tools & Manufacture,* **47**, 537–545.

Stephenson, D. & Agapiou, J. 2006. *Metal Cutting Theory and Practice 2nd Edition,* Boca Raton, Taylor and Francis.

Suh, S. H. & Lee, J. J. 1998. Five-axis part machining with three-axis CNC machine and indexing table. *Journal of Manufacturing Science and Engineering-Transactions of the ASME,* **120**, 120–128.

Tutunea-Fatan, O. R. & Feng, H. Y. 2004. Configuration analysis of five-axis machine tools using a generic kinematic model. *International Journal of Machine Tools & Manufacture,* **44**, 1235–1243.

Van Arnam, D. 1978. *Method for Forming Retroreflective Sheeting.* U.S. patent application 4243618. January 6, 1981.

Zeid, I. 2005. *Mastering CAD/CAM,* New York, McGraw-Hill.

CHAPTER 5

Development of a Postprocessor for Ultraprecise Single Point
Inverted Cutting of Right Triangular Prism Retroreflectors

5.1   Overview

In the previous chapter the postprocessor was introduced and discussed in brevity which does not give adequate understanding to its function, or potentially even its purpose. The following discussion is intended to give the reader sufficient knowledge of the purpose of a postprocessor and to thoroughly explain the function of the postprocessor developed for the fabrication of RTP arrays using the aforementioned USPIC strategies.

5.2   Introduction

Computer Aided Design (CAD) and Computer Aided Manufacturing (CAM) are used extensively throughout industry in an effort to reduce the time between product conception and realization. The design engineer creates a virtual model of the product by making use of a CAD system while the manufacturing engineer uses a CAM system to develop an appropriate manufacturing procedure and translate that procedure into machine tool language (Zeid, 2005). The virtual machine motions developed by the CAM system are written in a common generic language known as cutter location data (CL Data). The postprocessor then translates this to the numerical control (NC) programming language specific to machine tools – PMAC Script Language in this case. The postprocessor is not to be thought of as separate from the CAM system, rather it is an integral part of it. Because each machine tool differs by its kinematics and controller, each machine tool must have its own specific postprocessor (Apro, 2008).

The five-axis machine tool used throughout this project does have a postprocessor which can be applied to machining applications which make use of standard rotating tools and common toolpath strategies. The challenge at hand is that current CAM systems do not

support the toolpath and tooling of the USPIC cutting strategy. Therefore, the automation of writing G-Code for the fabrication of RTP structures was not possible, and manual writing was not feasible based on the number of lines necessary. To address this challenge, a program was developed in the MATLAB environment which automates the writing of the PMAC Script Language based on the previously discussed input parameters that specify both structure and array criteria.

5.3   Postprocessor

The flow of the program is outlined in the block diagram of Figure 5.1. Rectangles represent separate functions, parallelograms represent either an input or output, and rhombuses are conditional statements.
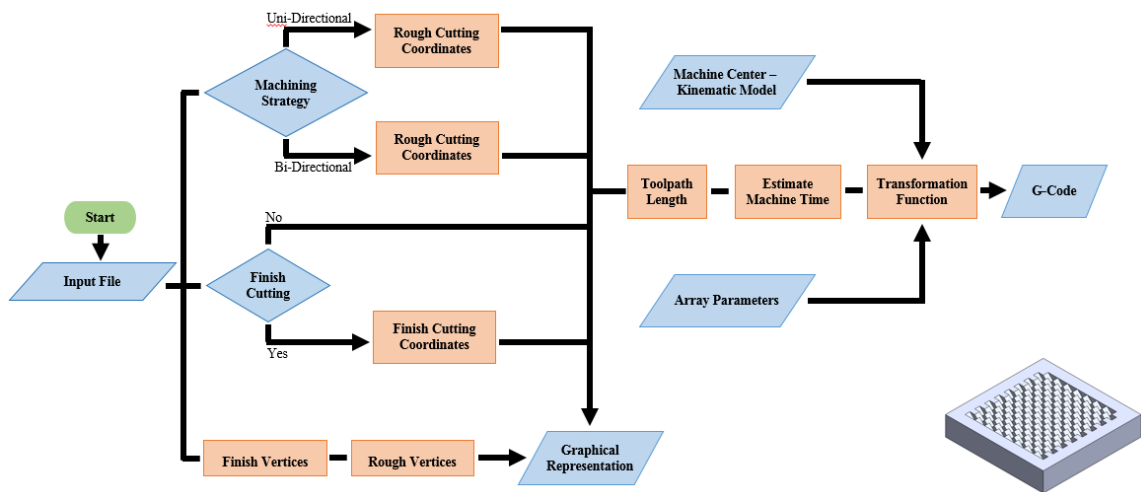
Figure 5.1 Block diagram of USPIC postprocessor

When the program is run, it first extracts variables from a text file – the input parameters. These include three parameters that determine the geometry of the RTP: *base*, *beta* and *width*, and eight parameters specific to the fabrication process: *strategy* (uni-directional, or bi-directional), *clearance height*, *roughing chip thickness*, *finishing chip thickness*, *number*

of finishing cuts (two in the case below), *length of chipbreaker* (applicable only to the uni-directional strategy), *rapid feed rate*, and *cutting feed rate* (Figure 5.2).
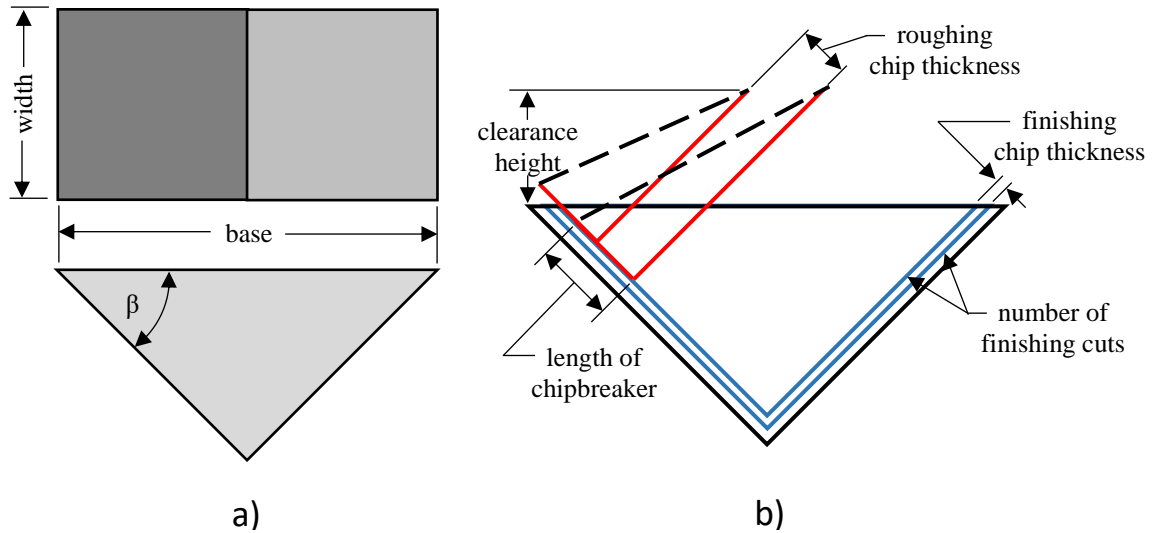
Figure 5.2 a) structure parameters, b) machining parameters

Clearance height is defined as a plane above, and parallel to, the workpiece which is determined as a "safe" distance for the tool to make ancillary motions at an increased traversing rate (*rapid feed rate*), and below this plane the tool should move at a slower rate conducive to cutting (*cutting feed rate*). This height is determined somewhat arbitrarily, but should be kept at a minimum for the sake of toolpath efficiency, while keeping the tool clear of the surface so as to reduce the likelihood of tool collisions.

Machining strategies can generally be divided into two procedures: roughing and finishing. The two procedures represent a tradeoff between material removal rate and resulting surface finish – the roughing procedure being focused on the rate of material removal, while the finishing strategy focuses on achieving optimal surface finish. The roughing procedure is carried out first and brings the geometry to a near finished state, after

which the finishing procedure removes the remaining material while achieving the desired surface finish.

Chip thickness, as referred to here, is defined as the thickness of the undeformed material being removed. Cutting conditions and material composition largely determine a preferred range for these two parameters, but Brinksmeier *et al.* has shown that a roughing and finishing thickness of 4 µm and 1–3 µm, respectively, produces consistent optical quality surface finish when using N37 as the workpiece material (Brinksmeier *et al.*, 2012). Brinksmeier *et al.* also applied a roughing feed rate of 45 mm/min and finishing feed rate of 3 mm/min.

Since cutting parameters rely primarily on the composition of the tool and workpiece, an experiment was carried out in order to determine what these parameters would ideally be for our specific application: a monocrystalline diamond tool, and a PMMA (poly methyl methacrylate) workpiece. This material was chosen because it is relatively soft when compared to metals, which will reduce the likelihood of tool damage during the verification phase of the USPIC strategy. Throughout the experiment, the resulting surface finish was observed for a series of 20 cuts in which the chip thickness was varied from 1 to 20 µm. The experiment was carried out three separate times – each with its own distinct applied feed rate (10, 50, and 100 mm/min). As a result, the cutting feed rate should be no more than 50 mm/min and the chip thickness less than 10 µm for the finishing cuts.

While a quantitative analysis of the resulting surface finish was not carried out, images of the cut surfaces were captured with a microscope. Six images are displayed in

Figure 5.3 below to give a general sense of how these two parameters affect the resulting surface finish. A comprehensive set of images was not deemed necessary for this discussion primarily for the sake of spatial constraints.

a)   b)   c)

d)   e)   f)
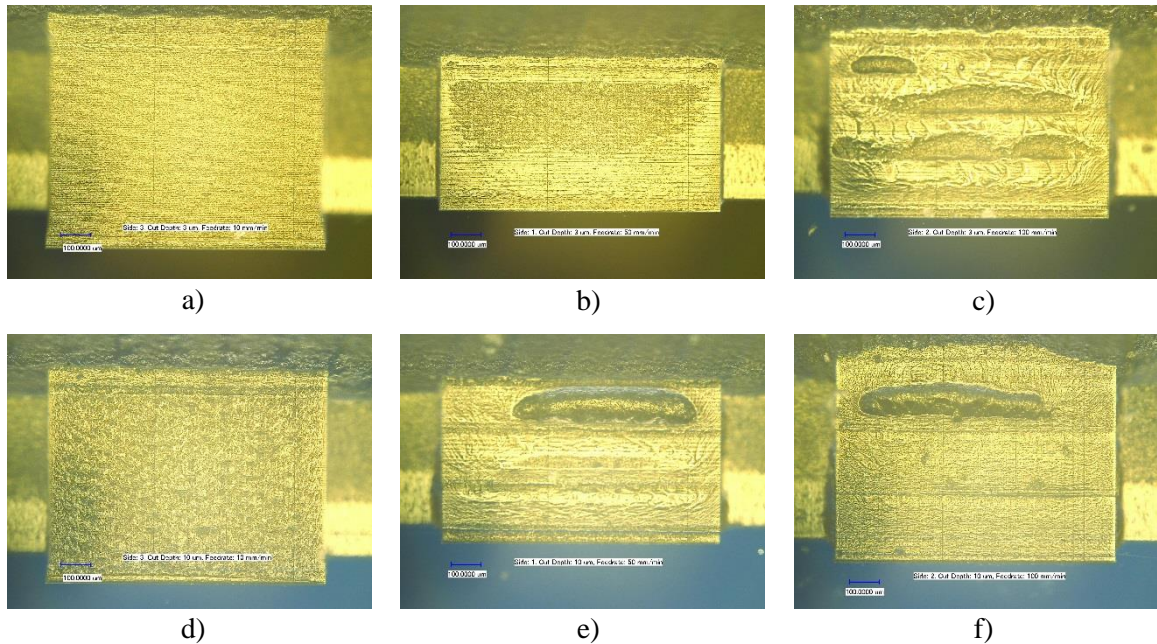
Figure 5.3 Qualitative surface roughness comparison: a) 3 µm at 10 mm/min, b) 3 µm at 50 mm/min, c) 3 µm at 100 mm/min, d) 10 µm at 10 mm/min, e) 10 µm at 50 mm/min, and f) 10 µm at 100 mm/min

Preliminary iterations of this program were carried out with a single finishing cut, but depending on the cutting conditions, this was often not enough to remove the poor surface finish left by the roughing strategy. Therefore, it was determined that the *number of finishing cuts* should be a variable. Finally, the *chipbreaker* is implemented in the uni-directional strategy as a means of separating the newly formed chip from the base material. Practically speaking, after the tool reaches the root of a cut the next motion is the chipbreaker which is along the adjacent facet. The length of this motion should be at least

the thickness of the chip being formed, but can be made longer in an effort to fully remove the chip from the cavity.

5.4   Rough Cutting Coordinates

Calculations for the cutting coordinates depend on the rough and finish vertices of the RTP structure, which are first determined based on the input parameters (Figure 5.4). Equations for each of these points utilize fundamental, right triangle trigonometry, a result of the RTP geometry, and were derived through examination.
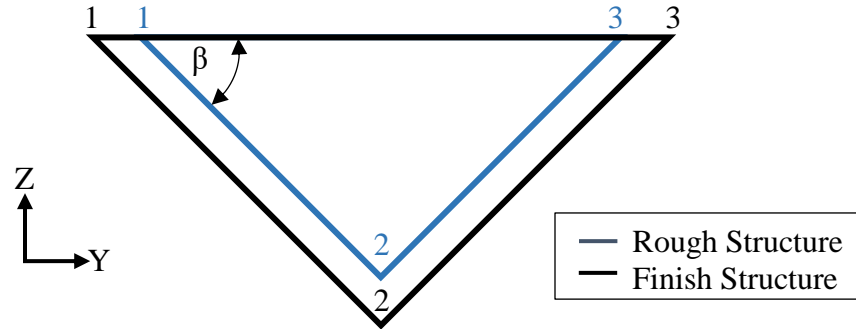
Figure 5.4 Finish and rough structure vertices

Finish structure coordinates are,

$$YF_1 = 0 \tag{5.1}$$

$$ZF_1 = 0 \tag{5.2}$$

$$YF_2 = base \cdot \cos^2(\beta) \tag{5.3}$$

$$ZF_2 = -base \cdot \cos(\beta) \cdot \sin(\beta) \tag{5.4}$$

$$YF_3 = base \tag{5.5}$$

$$ZF_3 = 0 \tag{5.6}$$

and rough structure coordinates are,

$$YR_1 = YF_1 + Fn \bullet FDOC / \sin(\beta) \tag{5.7}$$

$$ZR_1 = ZF_1 \tag{5.8}$$

$$YR_2 = YF_2 - Fn \bullet FDOC \bullet \sin(45 - \beta) / \sin(\beta) \tag{5.9}$$

$$ZR_2 = ZF_2 + Fn \bullet FDOC \bullet \cos(45 - \beta) / \sin(45) \tag{5.10}$$

$$YR_3 = YF_3 - Fn \bullet FDOC / \cos(\beta) \tag{5.11}$$

$$ZR_3 = ZF_3 \tag{5.12}$$

Where *Fn* is the number of finish cuts chosen by the user, and *FDOC* is the finishing depth of cut (*i.e.* chip thickness). *X* coordinates are all assumed to be zero which ensures the structure is aligned with the YZ plane.

Since the two roughing strategies differ in their respective cutting kinematics, it should follow that the cutting coordinates will also be different. Therefore, two separate MATLAB functions were written to calculate the roughing coordinates according to the strategy specified by the user. Equations for these coordinates were derived in a similar fashion to those of the structure vertices. It should also be noted that the coordinates for structure vertices and cutting coordinates are taken with respect to the corner of the RTP containing the angle *β*.

The uni-directional strategy is a repeated sequence of four motions: cutting, chipbreaker, and two ancillary motion. These four motions are linear interpolations between the points depicted in Figure 5.5 below. Parallel cuts are separated by the roughing chip thickness, *RDOC*. Since the length of the rough structure facet adjacent to β may not necessarily be divisible by an integer quantity of roughing cuts having a depth of cut equal to the desired roughing chip thickness, the exact value of this parameter is modified such that this condition becomes true. Maintaining a constant chip thickness throughout each procedure is an important detail which ensures the surface finish for each roughing cut can be accurately predicted.
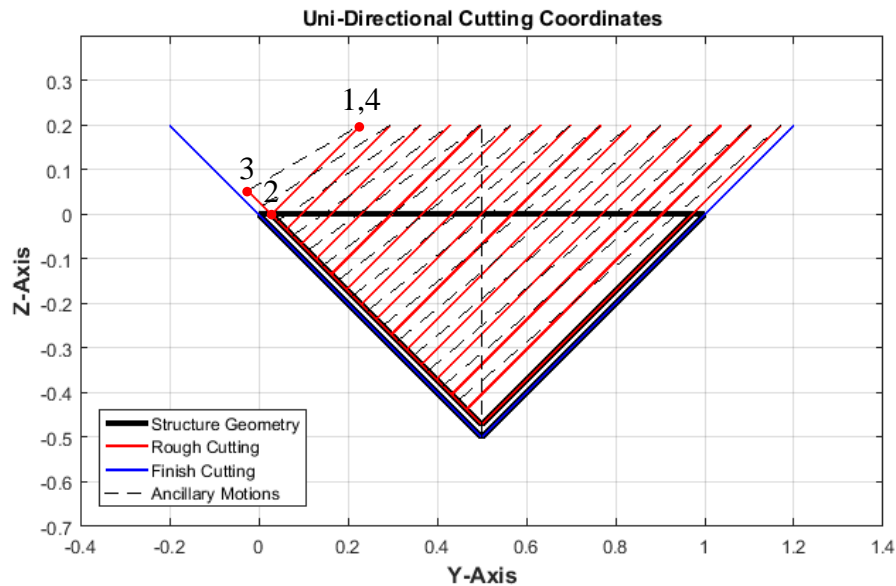
Figure 5.5 Graphical depiction of the uni-directional strategy

Coordinate calculations for the four points are,

$$Y_1 = YR_1 + ClearanceHeight \cdot \tan(\beta) \tag{5.13}$$

$$Z_1 = ZR_1 + ClearanceHeight \tag{5.14}$$

$$Y_2 = YR_1 \tag{5.15}$$

$$Z_2 = ZR_1 \tag{5.16}$$

$$Y_3 = YR_1 - Chipbreaker \bullet \cos(\beta) \tag{5.17}$$

$$Z_3 = ZR_1 + Chipbreaker \bullet \sin(\beta) \tag{5.18}$$

$$Y_4 = Y_1 \tag{5.19}$$

$$Z_4 = Z_1 \tag{5.20}$$

The remaining coordinates are calculated through a conditional statement, until the last set of four complete the geometry of the rough structure. Again, each set of four coordinates are separated by a distance equal to the modified value of the chip thickness as measured parallel to the facet adjacent to β.

The cutting coordinates for the bi-directional strategy are calculated in the same manner, but this strategy is a repeated sequence of six motions: two cutting, and four ancillary (Figure 5.6). It should be restated that this strategy relies on rotations about the Z-axis to ensure the tool is properly aligned with the facet being cut. These rotations are necessary after each cut is made and the tool is retracted to the clearance height – a total of two rotations for each sequence of six tool motions. In Figure 5.6 below, rotation occurs when the tool has reached position three and again at position six. These ancillary motions are not all depicted in Figure 5.6, doing so would only serve to increase the difficulty of interpretation.
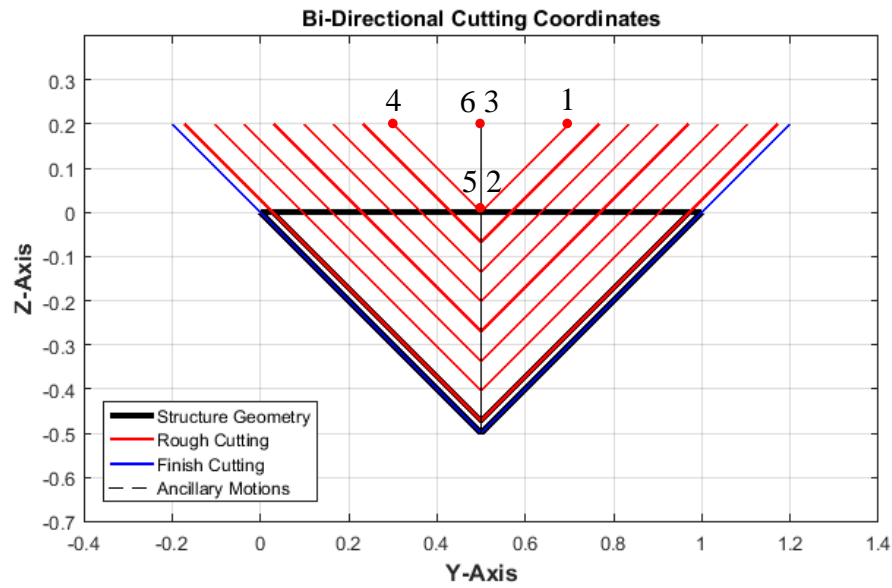
Figure 5.6 Graphical depiction of the bi-directional strategy

Coordinate calculations for the six points are then,

$$Y_1 = YD + ClearanceHeight \bullet \tan(\beta) \tag{5.21}$$

$$Z_1 = ZR_1 + ClearanceHeight \tag{5.22}$$

$$Y_2 = YD \tag{5.23}$$

$$Z_2 = ZR_1 \tag{5.24}$$

$$Y_3 = YD - ClearanceHeight / \tan(45 + \beta) \tag{5.25}$$

$$Z_3 = ZR_1 + ClearanceHeight \tag{5.26}$$

$$Y_4 = YD + ClearanceHeight \bullet \tan(90 - \beta) \tag{5.27}$$

$$Y_5 = YD \tag{5.28}$$

$$Z_5 = ZR_1 \tag{5.29}$$

$$Y_6 = YD - ClearanceHeight / \tan(45 + \beta) \tag{5.30}$$

$$Z_6 = ZR_1 + ClearanceHeight \tag{5.31}$$

Where YD is a point along the base of the geometry, which corresponds to a line originating from the vertex of the two facets and drawn at 45° from the same two facets. The line is necessary for this strategy in order to keep the number of cuts and their respective thickness identical for each facet. In the case of $\beta = 45°$ the line is vertical, but is at an angle for any other case. The present iteration of this program retracts the tool along this line after a cut, in an effort to reduce the likelihood of damaging the facet just cut.

Comparable to the uni-directional strategy, successive sequences of these six cuts are calculated with similar equations through a conditional statement which populates an array of cutting coordinates to be used in the generation of machine code written for the 5-axis CNC machine center employed for experiments.

5.5   Finish Cutting Coordinates

While many strategies could be conceived in order to complete the RTP geometry, the primary focus of the finishing procedure is to produce an optical quality surface finish (i.e. Ra < 10 nm). As a result of the experiment discussed in chapter three, it was determined that plough cutting is not capable of generating a surface finish comparable to that of

plunge cutting – a direct result of poor cutting angles (Figure 5.7). Therefore, the finish

cutting procedure should implement plunge cutting exclusively.

a)   b)
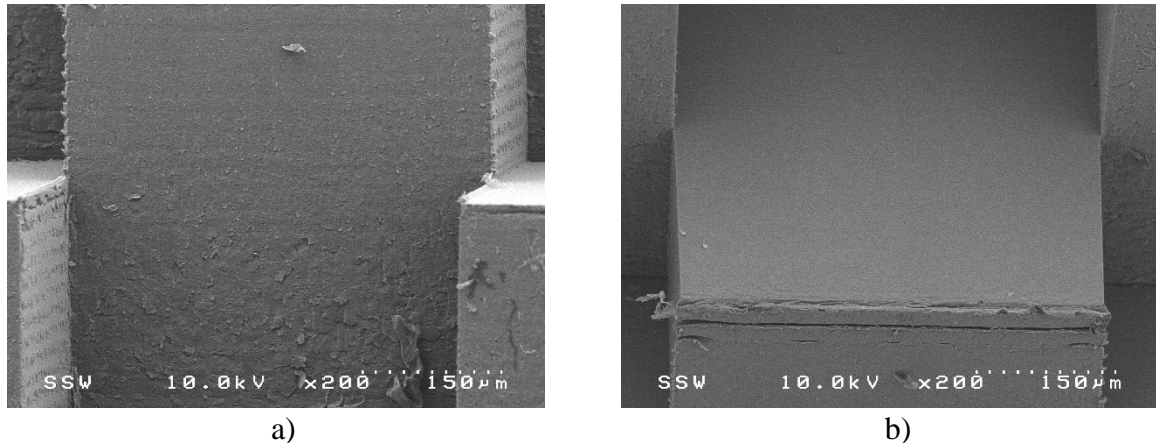
Figure 5.7 SEM images showing surface finish of reflective facets: a) plough cut facet,
b) plunge cut facet

The bi-directional strategy was developed in order to achieve the same criteria, so it is the

strategy applied to the finishing procedure, but differentiates itself from the bi-directional

roughing procedure by implementing a chip thickness and cutting feed rate specific to

finishing. Quantitatively speaking, both variables are generally less than those used in the

roughing procedure. Throughout experimentation, the finishing procedure used a chip

thickness and feed rate of 10 µm and 10 mm/min, respectively, whereas those for the

roughing procedure were 20 µm and 20 mm/min. Although the rapid feed rate for the two

procedures remained the same, the material removal rate for the finishing procedure can

be approximated as half that of the roughing procedure. For this reason, the number of

finishing cuts should be kept to a minimum in order to produce a sufficient surface finish

at an acceptable rate.

Throughout experimentation, between zero and three finishing cuts were used. The resulting surface finish from varying the number of cuts demonstrated that a minimum of two finishing cuts should be used following the uni-directional roughing strategy, while a single finishing cut is capable of producing the same results after the bi-directional strategy is used for roughing. Whatever the chosen number of finishing cuts may be, their coordinates are calculated and stored in an array similar to the method used for the roughing coordinates.

5.6   Kinematic Model/Transformation Function

The calculated coordinates could be applied to machining an RTP structure in a straightforward manner if the CNC machine in use was a 3-axis machine. In this case, a work offset vector would be used to establish the location of the workpiece with respect to the machine coordinate system (MCS) (Apro, 2008). This however is not the case when machining with rotational axes (She and Chang, 2007). Instead, the roughing and finishing coordinates, which are calculated with respect to the work coordinate system (WCS), must be transformed to the machine coordinate system (MCS). As mentioned in chapter four, the difficulty with this transformation is that the location and orientation of the WCS changes, with respect to the MCS, as the rotational axes index to the positions necessitated by the desired cutting kinematics. Therefore, it is necessary to translate the roughing and finishing coordinates from the WCS, which they were calculated relative to, to the MCS that the machine operates with respect to.

In chapter four the kinematic model and transformation function are discussed in detail for the machining of a single structure (Hamilton *et al.*, 2016). This discussion will

not reiterate that information, yet it is important to note that an additional vector was added

to the kinematic chain that describes the location of the RTP structure relative to the WCS

(Figure 5.8). This vector is necessary for the fabrication of a planar array of RTP structures

which each have their own X and Y coordinates describing their location within the array.

Therefore, the kinematic model of the machine now has an additional vector, and the

kinematic chain now starts at b_4 instead of the previous b_3.
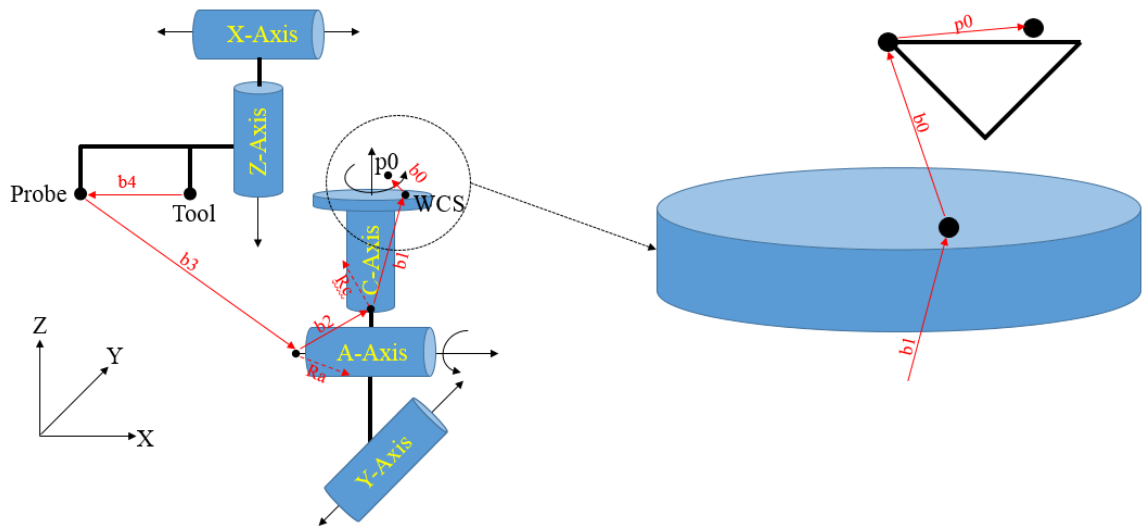
Figure 5.8 Kinematic model of precision 5-axis CNC machine

And the transformation function is now,

$$ {}^{M}_{W}[T] = b_4 \cdot b_3 \cdot R_x \cdot b_2 \cdot R_z \cdot b_1 \cdot b_0 \cdot p_0 \tag{5.32} $$

Where p_0 represents the roughing and finishing coordinates mentioned above. The

transformation equation is therefore a function of the XYZ coordinates of a single point in

the WCS, and the orientation of the A and C axes – with the output being the XYZ

coordinates of that point in the MCS. The transformed cutting coordinates are not stored in

an array, rather they are printed directly to a text file as machine code.

5.7   Machine Code

The final output in the block diagram of this postprocessor is a text file written in the appropriate language of the CNC machine which dictates the motions necessary to fabricate the desired array of RTP structures. This text file is synonymous with a program file for the machine and will be referred to as such throughout this discussion. The task of writing the program is handled by one of two MATLAB functions specific to each of the two cutting strategies: uni-directional and bi-directional. These two functions require the use of MATLAB's built in functions to create a text file and then read, and write to it.

The core of the program file is a series of X, Y, Z, A, and C coordinates which control the motion of the machine as it fabricates structures one-by-one. The actual strategy for machining arrays of RTP structures could take on many forms, but the structure-by-structure approach was chosen as a result of the development of the postprocessor. Primary iterations machined a single structure in order to verify the functionality of cutting strategies, so the natural progression to arrays applied this same approach. While machine time could likely be reduced through optimization, this was not pursued because of the time constraints of the project.

Lines of code are comprised of a single coordinate in the MCS, and the cutting tool moves in a linear fashion to each of the coordinates as it cuts the workpiece material. Machine functions such as feed rate, coolant control, and dwell time may also be controlled within the program, and comments may also be added according to the syntax required by the machine control.

A typical structure in an array requires hundreds of cutting coordinates and therefore hundreds of lines of code in the machine program. When a single structure is completed, the machine moves to the next location in the array and cuts another structure. This process is repeated until every structure in the array has been completed.

The postprocessor manages this structure-by-structure approach by using a nested logic loop. The outer loop is for the array coordinates while the inner loop handles cutting coordinates for each structure. The transformation function is used to calculate the MCS coordinates for each line of code as the logic loops step through their sequence. Each structure has its own array location, or b_0 vector, and each cutting coordinate its own location, or p_0 vector. In summary, the function transforms single structure cutting coordinates one-by-one, writes them to a text file, and repeats this for each structure in the array. The end result is many thousands of lines of code for a typical array.

5.8 Experimental Validation

This postprocessor was applied to the fabrication of a logo comprised of RTP structures (Figure 5.9). This particular logo was fabricated in order to demonstrate the postprocessor's ability to write machine code for nearly any two-dimensional array conceivable. Structures in the array below are characterized by a square aperture of 450 µm, and they are each aligned in a brick-like pattern with adjacent rows being offset by 50% of the structure length. The array was cut on a 0.5 mm thick, flat PMMA sheet. At the time of assembling this thesis, a quantitative assessment of the array was not completed; however, surface roughness and optical functionality will both be measured in the near future.

Figure 5.9 Fabricated logo comprised of RTP structures

5.9   Conclusion

Throughout the development of this postprocessor numerous tests were conducted in order to verify the function of each contributing component. Initially these tests were carried out with simulation software and later with the physical machine. The simulation software used was Vericut by CGTech which enables the user to simulate NC machine code without the risk of damaging machines and tooling. The software also allows for direct importing of CAD models to be used as machine components. Developing a CAD model of the 5-axis machine used throughout this project was the topic of previous work within the research group, so it was adopted as the simulation model for use in Vericut. The simulation phase of postprocessor verification proved quite useful for correcting miscalculations and logical errors.

The result of this work is an automated process for writing machine code specifically for the USPIC method. The toolpath length and machine time portions of the block diagram were intentionally excluded from this discussion because they do not play a

significant role in the postprocessor, and their description would not likely add value to the discussion.

In closing, many improvements to the postprocessor could be conceived for future studies. For instance, while some effort was focused on tool path optimization, the strategy applied to manufacturing arrays of RTP structures could be improved in an effort to reduce the number of rational and ancillary motions. Furthermore, typical automotive applications require retroreflective arrays described by freeform surfaces in order to follow the curvature of the vehicle; therefore, future iterations of this postprocessor should allow for arrays manufactured on freeform surfaces.

5.10 References

Apro, K. 2008. *Secrets of 5-Axis Machining,* New York, Industrial Press, Inc.

Brinksmeier, E., Glabe, R. & Schonemann, L. 2012. Diamond Micro Chiseling of large-scale retroreflective arrays. *Precision Engineering-Journal of the International Societies for Precision Engineering and Nanotechnology,* **36**, 650–657.

Hamilton, B., Milliken, N., Hussein, S., Tutunea-Fatan, O. R. & Bordatchev, E. V. 2016. Fabrication of Right Triangular Prism Retroreflectors through 3 1/2 1/2-Axis Ultraprecise Single Point Inverted Cutting. *Computer-Aided Design and Applications*.

She, C. H. & Chang, C. C. 2007. Design of a generic five-axis postprocessor based on generalized kinematics model of machine tool. *International Journal of Machine Tools & Manufacture,* **47**, 537–545.

Zeid, I. 2005. *Mastering CAD/CAM,* New York, McGraw-Hill.

CHAPTER 6

Discussion and Conclusions

6.1 Summary

The research conducted within this thesis contributes to the goal of developing a new and innovative manufacturing procedure for right triangular prism (RTP) retroreflectors. At the outset of this thesis no such research had been published, so it was not clear whether or not the RTP geometry was appropriate for retroreflection in automotive applications. To this end, the Ultraprecise Single Point Inverted Cutting technique (USPIC) has been proven applicable for the fabrication of two dimensional arrays of RTP structures.

The technique was envisioned as a combination of the mechanics of single point diamond turning, and the kinematics of multi-axis milling. As such, the tool developed for this technique resembles that of a standard grooving tool used in turning operations, and is fixed to an ultraprecise five-axis milling machine. Unlike common tools used in milling operations, the USPIC tool does not rotate during cutting. Instead, its cutting motion is provided by the linear axes of the milling machine.

Although many variations of cutting kinematics could be imagined, two techniques have been developed to produce the RTP geometry: the uni-directional, and bi-directional strategies. These represent a modification of classical cutting mechanics for single point operations (Stephenson and Agapiou, 2006). For instance, the tool geometry was developed in keeping with standard practices to allow for a straightforward prediction of material removal and generated surface finish. The first technique favours material removal over surface finish, while the second technique utilizes cutting mechanics that produce sufficient surface finish for both reflective facets, but requires additional ancillary motions – decreasing the material removal rate.

The additional ancillary motions necessitated by the bi-directional strategy require the use of the two rotational axes of the ultraprecise machine tool. These two axes are aligned with the X and Z principal axes of the machine, and allow for tool orientations otherwise not obtainable (Apro, 2008). However, the increased complexity of the machine kinematics, and novelty of the proposed cutting technique required the development of a suitable postprocessor whose foundation is a kinematic model of the machine.

As the rotary axes index throughout the bi-directional technique, the workpiece moves with it, so the orientation and location of the workpiece with respect to the machine coordinate system (MCS) are not immediately known. Therefore, its location and orientation must be calculated through a transformation function – a mathematical description of the kinematic model, which serves to simplify the job of the programmer by allowing for the translation of coordinate systems. Since the workpiece is a solid body, cutting coordinates can be calculated relative to a fixed location on the workpiece, or the workpiece coordinate system (WCS), and later converted to the MCS (Tutunea-Fatan and Feng, 2004).

In its current form, this postprocessor is able to produce machine code for the fabrication of two dimensional planar arrays of RTP structures. As seen in the experimental validation of chapter five, the solution is quite versatile and has been applied to simple arrays described by rectangular geometry, and more complex arrays described by familiar logos. Many of the fabricated arrays depicted in previous chapters required more than 50,000 lines of code – a result of the number of tool motions to complete a single structure.

6.2 Conclusions

Working in collaboration with the National Research Council of Canada (NRC), a new manufacturing technology has been developed – a viable option for the fabrication of RTP structures. The current iteration of this technique includes separate roughing and finishing procedures, each with process specific variables that provide for increased compatibility with workpiece materials and structure geometry. It also provides a means of automating the machine code writing process necessary to fabricate large arrays. Without an automated process, writing lines of code manually would be necessary but not feasible.

Throughout the development of this technique, visualization and simulation aids were also created. A CAD based macro was devised to generate RTP arrays, first for the purpose of visually analyzing changes to geometry, and second for the purpose of optical analysis with simulation software. As the research progressed toward physical experiments, a full CAD model of the five-axis machine, adapted from previous work, was used to verify and expose errors in the machine code writing process. This step proved invaluable, revealing small errors that would not have been easily identified throughout physical applications.

Initial quantitative analysis suggests that the RTP fabricated with USPIC outperforms the cube corner retroreflectors, and has a comparable optical performance to RTPs created with the pin-bundling technique (Hussein *et al.*, 2016). The geometry also lends itself to more straightforward toolpaths for the direct machining of structures. All things considered, the cutting technology developed herein not only serves to fill a literature gap in retroreflector technology, but also contributes to the advancement of the Canadian manufacturing sector.

6.2   Recommendations

Moving forward from the work presented in this thesis, a number of recommendations can be made to further develop the USPIC technology. A study of cutting mechanics should be conducted with a focus on optimizing process parameters. Currently, these parameters are chosen as a result of a parametric study in which surface finish was analyzed following incremental changes to the depth of cut and cutting speed. A better understanding of the mechanisms which affect surface finish would allow for the optimization of tool geometry and process parameters. Furthermore, the time intensive tool calibration procedure means that optical assessment of tool wear is an inconvenient and time intensive procedure. With a better understanding of cutting mechanics, tool life and wear predictions could be made.

The targeted surface finish of $R_a < 10$ nm was not achieved throughout testing which fundamentally limits optical functionality. This is believed to be a result of the PMMA workpiece material that was originally selected because of its machinability and optical clarity. Optimizing the cutting mechanics of this process may contribute to achieving the targeted surface finish. However, cutting RTP structures in a material suitable for moulding is a primary objective, and the process parameters and tool geometry developed for PMMA material are expected to change somewhat for mould materials, such as aluminum or tool steel.

Typical automotive applications require the surface of the retroreflective arrays to follow the lines and curves of the vehicle body which are by nature freeform. Further iterations of the postprocessor should therefore be focused on array parameters with the objective of producing arrays characterized by freeform surfaces. Intermediate steps should

include the ability to machine arrays on inclined and curved planes, as well as the ability to change the orientation of specific elements within the array.

Finally, a standard should be used, or developed, for the optical testing of samples. Automotive manufacturers must adhere to a standard set by the Society of Automotive Engineers (SAE, 2009). No such standard was applied for testing samples created with USPIC, which contributes to the difficulty of comparing fabricated samples with one another and with examples from automotive applications. Without this standard, the optical functionality of samples tends to be a subjective discussion rather than one based on quantitative results.

In closing, the current iteration of the USPIC technology provides a foundation for fabricating planar arrays of RTP structures with monocrystalline diamond tools and ultraprecise multi-axis milling machines. With regard to minimum structure size and machine time, this solution is an improvement over the pin-bundling technique. Further research should be carried out in order to develop this procedure to a point where it is capable of being adopted as a cost-efficient mass-fabrication alternative for automotive optical components.

6.3 References

Apro, K. 2008. *Secrets of 5-Axis Machining,* New York, Industrial Press, Inc.

Hussein, S., Hamilton, B., Tutunea-Fatan, O. R. & Bordatchev, E. V. 2016. Novel Retroreflective Micro-Optical Structure for Automotive Lighting Applications. *SAE International Journal of Passenger Cars – Mechanical Systems,* **9**.

SAE 2009. Reflex Reflectors. *Surface Vehicle Standard.* Warrendale, Pa.: Society of Automotive Engineers - International, 459–465.

Stephenson, D. & Agapiou, J. 2006. *Metal Cutting Theory and Practice 2nd Edition,* Boca Raton, Taylor and Francis.

Tutunea-Fatan, O. R. & Feng, H. Y. 2004. Configuration analysis of five-axis machine tools using a generic kinematic model. *International Journal of Machine Tools & Manufacture,* **44**, 1235–1243.

Curriculum Vitae

Name: Benjamin Hamilton

Post-secondary Fanshawe College
Education and   London, Ontario, Canada
Degrees   2007–2009 Certificate of Apprenticeship – General Machinist

        The University of Western Ontario
        London, Ontario, Canada
        2010–2014 B.E.Sc.

        The University of Western Ontario
        London, Ontario, Canada
        2014–2016 M.E.Sc.

Selected Honours Natural Sciences and Engineering Research Council of
and Awards: Canada – Alexander Graham Bell Canadian Graduate
        Scholarship
        2015–2016

Related Work   Teaching Assistant
Experience: The University of Western Ontario
        2014–2016

Publications:

1) **Hamilton, B.**, Hussein, S., Tutunea-Fatan, O.R., and Bordatchev, E.V., 2015, "Strategies in Single Point Inverted Cutting for Fabrication of Structured Surfaces," USB Proceedings of the 25th Canadian Congress of Applied Mechanics (CANCAM 2015), Jun. 2015, London, Canada, pp. 108–111.

2) Hussein, S., **Hamilton, B.**, Bordatchev, E.V., and Tutunea-Fatan, O.R., 2015, "Parameter-Driven Geometric Modeling of Retroreflective Features," USB Proceedings of the 25th Canadian Congress of Applied Mechanics (CANCAM 2015), Jun. 2015, London, Canada, pp. 96–99.

3) Hussein, S., **Hamilton, B.W.**, Bordatchev, E.V., and Tutunea-Fatan, O.R., 2016, "Optical Performance of Right Triangular Prism," Proceedings of the Photonics North 2016 Conference, May 2016, Quebec City, Canada.

4) **Hamilton, B.W.**, Hussein, S., Tutunea-Fatan, O.R., and Bordatchev, E.V., 2016, "Fabrication of Right Triangular Prism Retroreflectors Through Ultraprecise Single Point Inverted Cutting, Proceedings of the ASME Manufacturing Science and Engineering Conference 2016 (MSEC 2016), Jun. 2016, Blacksburg, USA, paper MSEC2016-8715, 11 pages.

5) Hussein, S., **Hamilton, B.W.**, Bordatchev, E.V., and Tutunea-Fatan, O.R., 2016, "Novel Retroreflective Micro-Optical Structure for Automotive Lighting Applications," SAE International Journal of Passenger Cars – Mechanical Systems, Vol. 9, Nr. 2, pp. 2016–2025.

6) **Hamilton, B.W.**, Milliken, N., Hussein, S., Tutunea-Fatan, O.R., and Bordatchev, E.V., 2016, "Fabrication of Right Triangular Prism Retroreflectors Through 3½½-Axis Ultraprecise Single Point Inverted Cutting," accepted for publication in Computer-Aided Design and Applications.